

## Diplomarbeit

# Channel Estimation for UMTS Long Term Evolution

Ausgeführt zum Zwecke der Erlangung des akademischen Grades eines  
Diplom-Ingenieurs unter Leitung von

Univ.Prof. Dipl.-Ing. Dr.techn. Markus Rupp

Dipl.-Ing. Christian Mehlführer

Dipl.-Ing. Martin Wrulich

E389

Institut für Nachrichtentechnik und Hochfrequenztechnik

eingereicht an der Technischen Universität Wien

Fakultät für Elektrotechnik und Informationstechnik

von

**Michal Šimko**

Matrikelnr.: 0425054

Kulíšková 19, 821 08 Bratislava, Slowakei

Vienna, June 2009

.....

I certify that the work presented in this diploma thesis was done by myself  
and the work of other authors is properly cited.

*Michal Šimko*  
*Vienna, June 2009*

# Abstract

In this master thesis, I discuss the problem of channel estimation for Long Term Evolution (LTE). LTE uses coherent detection, that requires channel state information. LTE provides training data for channel estimation. To assess the performance of different channel estimators, I utilize the LTE link level simulator developed at the Institute of Communications and Radio-Frequency Engineering (INTHFT), Vienna University of Technology. The channel estimators are compared in terms of throughput of the complete system for slowly and rapidly changing channels. The Least Squares (LS) channel estimator with linear interpolation is losing 2 dB, and the Linear Minimum Mean Square Error (LMMSE) channel estimator 0.5 dB with respect to the system with perfect channel knowledge. In order to reduce the complexity, while preserving the performance of the LMMSE channel estimator, Approximate Linear Minimum Mean Square Error (ALMMSE) channel estimators are also investigated. I present implementations of such an approximate channel estimator for slowly changing channels and for rapidly changing channels. The ALMMSE estimator for block fading uses the correlation between the  $L$  closest subcarriers. In the fast fading case, the ALMMSE estimator utilizes the structure of the channel autocorrelation matrix. Furthermore, this thesis shows some simulations, from which the block fading assumption can be proofed valid for velocities up to approximately 20 km/h. At higher velocities, the subcarriers are not perfectly orthogonal to each other. Thus, Inter Carrier Interference (ICI) occurs. At higher velocities, the Signal to Interference and Noise Ratio (SINR) should be considered instead of Signal to Noise Ratio (SNR).

# Contents

<b>1</b>	<b>Introduction</b>	<b>1</b>
<b>2</b>	<b>LTE Downlink: Physical Layer</b>	<b>3</b>
2.1	Overview . . . . .	3
2.2	Structure of Pilot Symbols . . . . .	4
2.3	System Model . . . . .	5
<b>3</b>	<b>Channel Estimation for Block Fading</b>	<b>11</b>
3.1	Least Squares Channel Estimation . . . . .	12
3.2	Linear Minimum Mean Square Error Channel Estimation . . .	15
3.2.1	LMMSE Channel Estimation for Spatially Uncorrelated Channels . . . . .	16
3.2.2	LMMSE Channel Estimation for Spatially Correlated Channels . . . . .	17
3.3	Approximate LMMSE Channel Estimation . . . . .	18
3.4	Simulation Results . . . . .	21
3.4.1	Comparison of Interpolation Techniques . . . . .	22
3.4.2	LMMSE Channel Estimation . . . . .	24
3.4.3	ALMMSE Channel Estimation . . . . .	28
<b>4</b>	<b>Channel Estimation for Fast Fading</b>	<b>34</b>
4.1	Least Square Channel Estimation . . . . .	34
4.2	Linear Minimum Mean Square Error Channel Estimation . . .	35
4.3	Approximate LMMSE Channel Estimation . . . . .	37
4.4	Simulation Results . . . . .	40
4.4.1	Comparison of Fast Fading Channel Estimation . . . . .	41
4.4.2	Block Fading Channel Estimation . . . . .	43
4.4.3	ALMMSE Channel Estimation . . . . .	48
<b>5</b>	<b>Conclusions and Further Work</b>	<b>50</b>
<b>A</b>	<b>Acronyms</b>	<b>52</b>
	<b>Bibliography</b>	<b>53</b>

# List of Figures

2.1	Signal structure . . . . .	4
2.2	Pilot symbols structure . . . . .	6
2.3	System Model . . . . .	7
3.1	Example of linear interpolation . . . . .	14
3.2	Comparison of interpolation techniques for one channel realization . . . . .	16
3.3	Principle of the ALMMSE estimator . . . . .	19
3.4	MSE for different interpolation techniques . . . . .	22
3.5	Throughput for different interpolation techniques . . . . .	23
3.6	MSE for the linear interpolation over subcarrierindex and SNR	24
3.7	MSE for the sinc interpolation in the frequency domain over subcarrierindex and SNR . . . . .	25
3.8	MSE for the LMMSE estimator versus the LS estimator . . . .	26
3.9	Throughput for the LMMSE estimator versus the LS estimator	26
3.10	MSE for the LMMSE estimator with estimated autocorrelation matrix . . . . .	28
3.11	Throughput for the LMMSE estimator with estimated autocorrelation matrix . . . . .	29
3.12	MSE for the LMMSE estimator with estimated autocorrelation matrix over M . . . . .	30
3.13	Throughput for the LMMSE estimator with estimated autocorrelation matrix over M . . . . .	30
3.14	MSE for the LMMSE estimator for spatially correlated channels	31
3.15	Throughput for the LMMSE estimator for spatially correlated channels . . . . .	31
3.16	MSE for the ALMMSE estimator with different L . . . . .	32
3.17	Throughput for the ALMMSE estimator with different L . . . .	32
3.18	SNR loss of the ALMMSE estimator to the LMMSE estimator over L . . . . .	33
4.1	Example of a fast fading channel . . . . .	41

4.2	MSE for different fast fading estimators . . . . .	42
4.3	Throughput for different fast fading estimators . . . . .	43
4.4	MSE for the LMMSE estimator using wrong temporal statistics	44
4.5	Throughput for the LMMSE estimator using wrong temporal statistics . . . . .	44
4.6	MSE for block fading estimator applied on fast fading scenario	45
4.7	Throughput for block fading estimator applied on fast fading scenario . . . . .	46
4.8	Inter carrier interference power . . . . .	47
4.9	SNR/SINR mapping for a moving UE . . . . .	47
4.10	MSE for the ALMMSE estimator . . . . .	48
4.11	Throughput for the ALMMSE estimator . . . . .	49

# List of Tables

3.1	Simulator settings for block fading simulations . . . . .	21
3.2	SNR loss of different Interpolation techniques to the system with perfect channel knowledge . . . . .	24
4.1	Simulator settings for fast fading simulations . . . . .	40

# Chapter 1

## Introduction

Approximately every ten years, there is a new standard for mobile communication. Analog mobile phone systems were introduced in 1981, the Global System for Mobile communications (GSM) in 1991, Wideband Code Division Multiple Access (W-CDMA) in 2001, and Long Term Evolution (LTE) will be most likely commercially launched in 2010 [1]. The analog system enabled people to carry their own cell phones and make phone calls on the move. GSM brought more security and some new services like Short Message Service (SMS), Wireless Application Protocol (WAP), etc. This was a time of great changes in society, as well as a time of rapid increase of cell phone users. Suddenly, a business could be done on the move. Everything got faster. The youth started to interact via SMS. People got closer, at least in some sense. The W-CDMA standard increased the connection speed which allowed to make video calls, browse the internet from anywhere, and other mobile applications. However, this influence was not so tremendous as ten years before. In contrast to the prediction, the people did not use video calling. Maybe some of them did not even realize, that their cell phones worked on a different basis. Not just the technical perfection of a standard, but also the offered services make a standard successful.

Today, the market of cell phones is shrinking [2], and a new global standard is on the horizon. Still, two open question are remaining. First, how to use the wireless "broadband"? High speed connection without proper services is useless. Will LTE bring new changes to the society, or is telephony, SMS and internet browsing everything, that the mobile communication can offer us? Secondly, what will happen in the next ten, twenty years? Are we just going to increase the connection speed, or will we be able to offer society something new, something, what will move us in the right direction?



In my master thesis, I concentrate on the close future. I investigate channel estimation for LTE, necessary for coherent detection, which will be used by every LTE device. Thus, it is important to analyse this topic. The estimators are compared by means of the throughput, that allows to observe influence of an estimator on the complete system. Although the Mean Square Error (MSE) shows directly the performance of an estimator, it is not clear if the decrease of MSE, will also increase the throughput. I discuss channel estimators for rapidly changing channels, where the subcarriers are not perfectly orthogonal to each other. I present two approximations of the Linear Minimum Mean Square Error (LMMSE) channel estimator, which are relevant for real-time applications due to their performance and their low complexity.

The thesis is organized as follows: In Chapter 2, I present the important facts about LTE from a channel estimation point of view. I also introduce a mathematical system model. In Chapter 3, I discuss channel estimation for slowly changing channels. This analysis is extended in Chapter 4 to rapidly changing channels. Finally, in Chapter 5, I summarize my thesis.

## Chapter 2

# LTE Downlink: Physical Layer

LTE is a project within 3rd Generation Partnership Project (3GPP), which will be introduced in Release 8. More details on LTE can be found in [3]. In the following chapter, I will present LTE characteristics, which are relevant from a channel estimation point of view. Furthermore, I will present the system model, which is used in this work.

### 2.1 Overview

The LTE downlink is based on Orthogonal Frequency Division Multiplexing (OFDM), which is an attractive downlink transmission scheme due to its robustness against frequency selective channels. LTE supports the use of multiple transmit and receive antennas, and uses different modulation alphabets and channel codes according to the signalized channel quality. Furthermore, the time-frequency resources are dynamically shared between users. Adaptive modulation and coding, support of Multiple Input Multiple Output (MIMO) and Hybrid Automated Repeat Request (H-ARQ) are the prime keystones of the LTE downlink.

At the highest level, the LTE signal in the time domain consists of frames of duration  $T_{\text{frame}} = 10 \text{ ms}$ , which themselves consists of ten equally long subframes with  $T_{\text{subframe}} = 1 \text{ ms}$ . Each subframe comprises two equally long slots of duration  $T_{\text{slot}} = 0.5 \text{ ms}$ . Each slot consists of a number of OFDM symbols (six or seven) with cyclic prefix. LTE defines two different cyclic prefix length, normal and extended. In Figure 2.1, the signal structure for normal cyclic prefix length is depicted. According to the used bandwidth, each OFDM symbol consists of a number of subcarriers. Subcarriers are grouped into resource blocks, where each resource block consists of 12 adja-

cent subcarriers, with 15 kHz spacing between two consecutive subcarriers. LTE allows to use any number of resource blocks from 6 up to 100, which corresponds to bandwidth from 1.4 MHz up to 20 MHz.

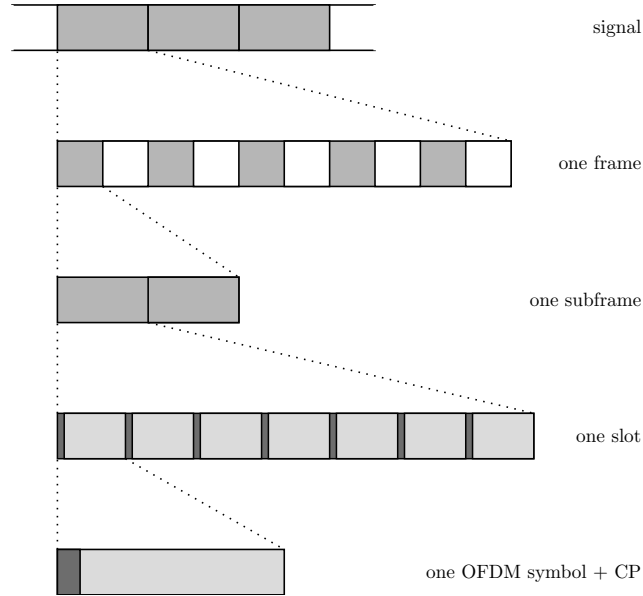


Figure 2.1: Signal structure

## 2.2 Structure of Pilot Symbols

To enable coherent demodulation, channel estimation is required. A simple way to enable channel estimation in an OFDM system is to insert known pilot symbols into the time-frequency grid of the transmit signal. The position of the pilot symbols depends on the number of transmit antenna ports [3]. Whenever, there is a pilot symbol located within the time-frequency grid at one transmit antenna port, the symbols at same position at the remaining transmit antenna ports are 0. Figure 2.2 depicts structure of the pilot symbols for 4 transmit antenna ports. The colored squares correspond to the pilot symbols at a particular antenna port and crosses corresponds to positions within time-frequency grid, which are 0. Within each resource block at 1st and 2nd transmit antenna port, there are 4 pilot symbols, and at the 3rd and 4th transmit antenna port just 2. It is obvious, that with increasing number of antennas, the number of pilot symbols and symbols, which are 0, is increasing. This fact results in decreasing spectral efficiency with increasing number of transmit antenna ports (e.g. in case of 4 transmit

antenna ports, 14.3% of all symbols is used just for channel estimation). At the 3rd and 4th transmit antenna ports, less pilot symbols than at the 1st and 2nd transmit antenna ports are located. Therefore, in general the quality of the channel estimates from 3rd and 4th transmit antenna ports will be poorer, than the quality of channel estimate from 1st and 2nd transmit antenna port. Consequently, the use of 4 transmit antenna ports should be restricted to scenarios, in which the channel is not changing rapidly [4].

The complex value of the pilot symbols will vary between different pilot symbol positions and also between different cells. Thus, the reference signal can be seen as two dimensional cell identifier sequence. In [3], 510 different cell identities (170 cell identity groups and 3 specific cell identity within one cell identity group) are defined. Thus, the complex value of pilot symbols is cell dependent. The frequency domain position of the pilot symbols may vary between consecutive subframes. The relative position of the pilot symbols is always the same, as depicted in Figure 2.2. The frequency hopping can be described as adding frequency offset to the basis pilot symbols position structure. There are 170 hopping pattern defined, where each corresponds to one cell identity group.

## 2.3 System Model

The relevant components of the considered system are depicted in Figure 2.3. In the following mathematical description just one subframe is considered and for sake of simplicity the subframe index will be omitted. At the transmitter, the data bits of one subframe are generated (in the complete system these data bits are scrambled and encoded, but from channel estimation point of view this is of minor importance). Before serial-to-parallel conversion, the symbols are modulated according to [3] and pilot symbols are inserted. After Inverse Fast Fourier Transform (IFFT) and parallel-to-serial conversion, the cyclic prefix is inserted and the transmit signal is generated by a Digital-to-analog converter. At the receiver, the cyclic prefix is removed. Using Fast Fourier Transform (FFT), the signal is converted into the frequency domain. Using the channel estimation and equalization, the data estimates are obtained.

The following system model is based on [5]. Let  $\mathbf{x}_{d,n_t}^{(f)}$  be a length  $N_d$  column vector comprising all modulated data symbols of one subframe in the frequency domain (indicated by (f)) at the transmit antenna port  $n_t$  ( $n_t = 1 \cdots N_t$ ). Furthermore, let  $\mathbf{x}_{p,n_t}^{(f)}$  be a length  $N_p$  column vector com-

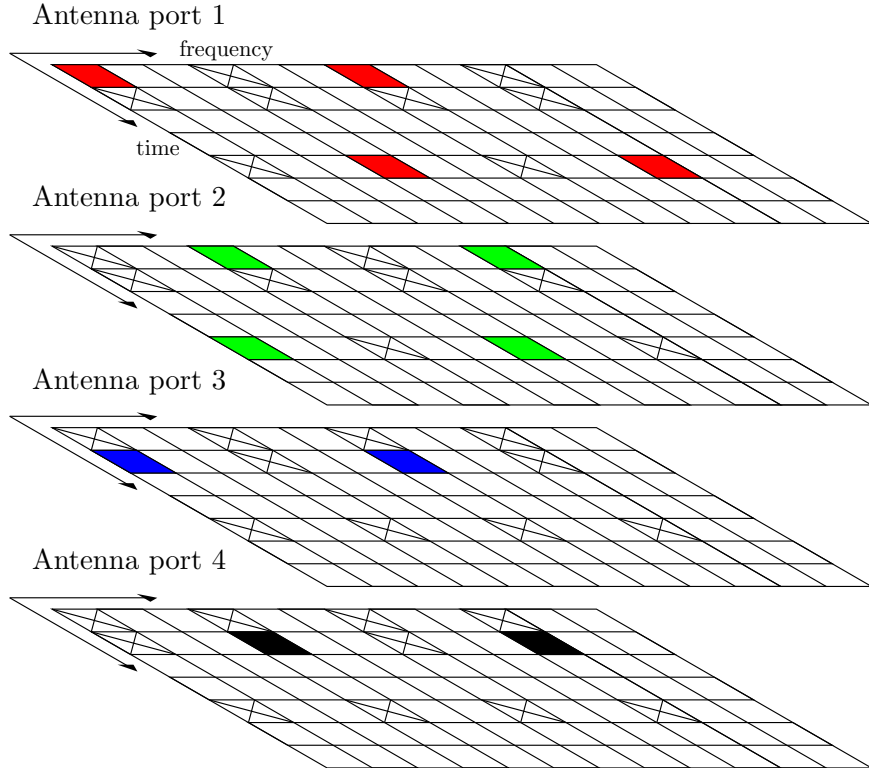


Figure 2.2: Pilot symbols structure

prising all pilot symbols. Let vector  $\tilde{\mathbf{x}}_{n_t}$  be the concatenation of vector  $\mathbf{x}_{p,n_t}^{(f)}$  and vector  $\mathbf{x}_{d,n_t}^{(f)}$

$$\tilde{\mathbf{x}}_{n_t}^{(f)} = \begin{bmatrix} \mathbf{x}_{p,n_t}^{(f)T} & \mathbf{x}_{d,n_t}^{(f)T} \end{bmatrix}^T. \quad (2.1)$$

After permuting the vector  $\tilde{\mathbf{x}}_{n_t}^{(f)}$  with a permutation matrix  $\mathbf{P}$  that fulfills  $\mathbf{P}^T \mathbf{P} = \mathbf{P} \mathbf{P}^T = \mathbf{I}$ , a column vector  $\mathbf{x}_{n_t}^{(f)}$  of length  $N_p + N_d$  is obtained

$$\mathbf{x}_{n_t}^{(f)} = \mathbf{P} \tilde{\mathbf{x}}_{n_t}^{(f)}. \quad (2.2)$$

The vector  $\mathbf{x}_{n_t}^{(f)}$  consists of  $N_s$  OFDM symbols

$$\mathbf{x}_{n_t}^{(f)} = \begin{bmatrix} \mathbf{x}_{n_t,0}^{(f)T} & \dots & \mathbf{x}_{n_t,N_s-1}^{(f)T} \end{bmatrix}^T. \quad (2.3)$$

The  $n_s$ -th OFDM symbol is represented by the vector  $\mathbf{x}_{n_t,n_s}^{(f)}$  of length  $K_{\text{sub}}$

$$\mathbf{x}_{n_t,n_s}^{(f)} = \begin{bmatrix} x_{n_t,n_s,0}^{(f)} \dots x_{n_t,n_s,K_{\text{sub}}-1}^{(f)} \end{bmatrix}^T \quad (2.4)$$

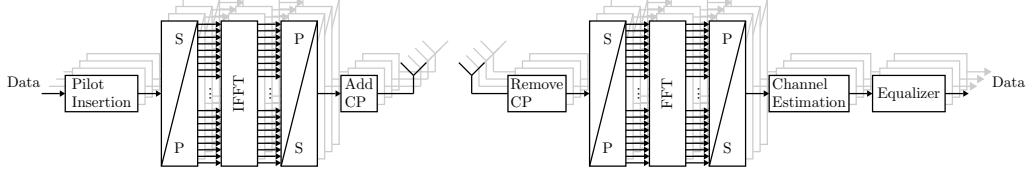


Figure 2.3: System Model

in which the elements  $x_{n_t, n_s, k}^{(f)}$  correspond to the symbols at the  $n_t$ -th transmit antenna port within the  $n_s$ -th OFDM symbol on the  $k$ -th subcarrier. The transmit signal of the  $n_s$ -th OFDM symbol in the time domain, indicated by  $(t)$ , can be written as

$$\mathbf{x}_{n_t, n_s}^{(t)} = \mathbf{F}_{\text{CP}} \mathbf{D}_{K_{\text{FFT}}}^H \mathbf{F}_{\text{guard}} \mathbf{x}_{n_t, n_s}^{(f)}. \quad (2.5)$$

where  $\mathbf{F}_{\text{guard}}$  indicates an  $K_{\text{FFT}} \times K_{\text{sub}}$  matrix adding  $(K_{\text{FFT}} - K_{\text{sub}})$  zero symbols on guard subcarriers. The matrix  $\mathbf{D}_{K_{\text{FFT}}}$  the Discrete Fourier Transform (DFT) matrix and  $\mathbf{F}_{\text{CP}}$  is a matrix, which adds cyclic prefix to the OFDM symbol in the time domain. The matrix  $\mathbf{F}_{\text{guard}}$  is defined as

$$\mathbf{F}_{\text{guard}} = \begin{pmatrix} \mathbf{I}_{K_{\text{sub}}} \\ \mathbf{0}_{(K_{\text{FFT}} - K_{\text{sub}}) \times K_{\text{sub}}} \end{pmatrix} \quad (2.6)$$

with  $\mathbf{I}_z$  being the  $z \times z$  identity matrix, and  $\mathbf{0}$  denotes a zero matrix of a given dimension. Furthermore,  $\mathbf{D}_{K_{\text{FFT}}}$  is the DFT matrix of dimension  $K_{\text{FFT}} \times K_{\text{FFT}}$  with elements  $\frac{1}{\sqrt{L}} e^{-j \frac{2\pi}{K_{\text{FFT}}} i_r i_c}$  ( $i_r$  and  $i_c$  are the row and column indices, respectively).  $\mathbf{F}_{\text{CP}}$  is an  $(K_{\text{FFT}} + P) \times K_{\text{FFT}}$  matrix adding a cyclic prefix of length  $P$  to a vector of length  $K_{\text{FFT}}$ , which is defined as

$$\mathbf{F}_{\text{CP}} = \begin{pmatrix} \mathbf{0}_{P \times (K_{\text{FFT}} - P)} & \mathbf{I}_P \\ \mathbf{I}_{K_{\text{FFT}}} \end{pmatrix}. \quad (2.7)$$

At the receiver, after Analog/Digital (A/D) conversion, the receive signal of the  $n_s$ -th OFDM symbol in the time domain at receive antenna port  $n_r$  is obtained as

$$\mathbf{y}_{n_r, n_s}^{(t)} = \sum_{n_t=1}^{N_t} \mathbf{H}_{n_t, n_r, n_s}^{(t)} \mathbf{x}_{n_t, n_s}^{(t)} + \mathbf{w}_{n_r, n_s}^{(t)} \quad (2.8)$$

where  $\mathbf{y}_{n_r, n_s}^{(t)}$  is the  $n_s$ -th received OFDM symbol in the time domain of length  $K_{\text{FFT}} + P$ ,  $\mathbf{H}_{n_t, n_r, n_s}^{(t)}$  is the channel matrix between the  $n_t$ -th transmit and  $n_r$ -th receive antenna port and  $\mathbf{w}_{n_r, n_s}^{(t)}$  is the noise vector, which elements are considered to be white Gaussian zero mean random variables with variance  $\sigma_w^2$ . The channel matrix  $\mathbf{H}_{n_t, n_r, n_s}^{(t)}$  is a toeplitz matrix of dimension  $(K_{\text{FFT}} + P) \times (K_{\text{FFT}} + P)$  with the following structure. Here, I assume that the channel impulse response has at most  $N_h$  taps and for sake of simplicity, I also omitted the antenna port indices.

$$\mathbf{H}_{n_s}^{(t)} = \begin{bmatrix} h_{n_s, 0}^{(t)} & 0 & \dots & \dots & \dots & 0 \\ \vdots & \ddots & \ddots & & & \vdots \\ h_{n_s, N_h - 1}^{(t)} & & \ddots & \ddots & & \vdots \\ 0 & \ddots & & \ddots & \ddots & \vdots \\ \vdots & \ddots & \ddots & & \ddots & 0 \\ 0 & \dots & 0 & h_{n_s, N_h - 1}^{(t)} & \dots & h_{n_s, 0}^{(t)} \end{bmatrix} \quad (2.9)$$

where  $h_{n_s, n_h}^{(t)}$  is a tap of the channel impulse response with delay  $n_h$  of the  $n_s$ -th OFDM symbol. Here, I assumed that the channel impulse response is constant over duration of a OFDM symbol. If this assumption is violated, Inter Carrier Interference (ICI) will occur. If the channel is time variant, the columns of the matrix  $\mathbf{H}_{n_s}^{(t)}$  are time dependent, which is trivial extension to Equation (2.9).

At the receiver, the cyclic prefix is removed, FFT is performed, and at last the guard symbols are removed

$$\mathbf{y}_{n_r, n_s}^{(f)} = \mathbf{F}_{\text{guard,rem}} \mathbf{D}_{K_{\text{FFT}}} \mathbf{F}_{\text{CP,rem}} \mathbf{y}_{n_r, n_s}^{(t)} \quad (2.10)$$

where  $\mathbf{F}_{\text{CP,rem}}$  performs the cyclic prefix removal and is of dimension  $K_{\text{FFT}} \times (K_{\text{FFT}} + P)$  with the following structure

$$\mathbf{F}_{\text{CP,rem}} = \begin{pmatrix} \mathbf{0}_{K_{\text{FFT}} \times P} & \mathbf{I}_{K_{\text{FFT}}} \end{pmatrix}. \quad (2.11)$$

$\mathbf{F}_{\text{guard,rem}}$  is an  $K_{\text{sub}} \times K_{\text{FFT}}$  matrix, which removes the guard subcarriers. The matrix  $\mathbf{F}_{\text{guard,rem}}$  is defined as

$$\mathbf{F}_{\text{guard,rem}} = \begin{pmatrix} \mathbf{I}_{K_{\text{sub}}} & \mathbf{0}_{K_{\text{sub}} \times (K_{\text{FFT}} - K_{\text{sub}})} \end{pmatrix}. \quad (2.12)$$

After removing the cyclic prefix, performing the FFT and removal of the guard band, Equation (2.8) can be equivalently rewritten as

$$\mathbf{y}_{n_r, n_s}^{(f)} = \sum_{n_t=1}^{N_t} \mathbf{\Lambda}_{n_t, n_r, n_s}^{(f)} \mathbf{x}_{n_t, n_s}^{(f)} + \mathbf{w}_{n_r, n_s}^{(f)} \quad (2.13)$$

where  $\mathbf{y}_{n_r, n_s}^{(f)}$  is the  $n_s$ -th received OFDM symbol in the frequency domain, and  $\mathbf{\Lambda}_{n_t, n_r, n_s}^{(f)}$  is an  $K_{\text{sub}} \times K_{\text{sub}}$  channel matrix between the  $n_t$ -th and  $n_r$ -th antenna port, which is obtained as

$$\mathbf{\Lambda}_{n_t, n_r, n_s}^{(f)} = \mathbf{F}_{\text{guard,rem}} \mathbf{D}_{K_{\text{FFT}}} \mathbf{F}_{\text{CP,rem}} \mathbf{H}_{n_t, n_r, n_s}^{(t)} \mathbf{F}_{\text{CP}} \mathbf{D}_{K_{\text{FFT}}}^H \mathbf{F}_{\text{guard}}. \quad (2.14)$$

If the channel is not changing over the duration of one subframe, the matrix  $\mathbf{\Lambda}_{n_t, n_r, n_s}^{(f)}$  is diagonal. The vector  $\mathbf{w}_{n_r, n_s}^{(f)}$  is the noise in the frequency domain. Let  $\mathbf{h}_{n_t, n_r, n_s}^{(f)}$  denote a length  $K_{\text{sub}}$  vector comprising diagonal elements of the matrix  $\mathbf{\Lambda}_{n_t, n_r, n_s}^{(f)}$  and  $\mathbf{h}_{n_t, n_r}^{(f)}$  the concatenation of  $N_s$  channel vectors  $\mathbf{h}_{n_t, n_r, n_s}^{(f)}$

$$\mathbf{h}_{n_t, n_r}^{(f)} = \left[ \mathbf{h}_{n_t, n_r, 0}^{(f)T} \cdots \mathbf{h}_{n_t, n_r, N_s-1}^{(f)T} \right]^T. \quad (2.15)$$

By permutation of  $\mathbf{h}_{n_t, n_r}^{(f)}$  analog to Equation (2.1), the same structure of the channel vector can be obtained

$$\tilde{\mathbf{h}}_{n_t, n_r}^{(f)} = \mathbf{P}^T \mathbf{h}_{n_t, n_r}^{(f)} = [\mathbf{h}_{p, n_t, n_r}^{(f)T} \mathbf{h}_{d, n_t, n_r}^{(f)T}]^T. \quad (2.16)$$

Let vector  $\mathbf{y}_{n_r}^{(f)}$  be a connection of  $N_s$  received OFDM symbols from the  $n_r$ -th receiver antenna port

$$\mathbf{y}_{n_r}^{(f)} = \left[ \mathbf{y}_{n_r, 0}^{(f)T} \cdots \mathbf{y}_{n_r, N_s-1}^{(f)T} \right]^T \quad (2.17)$$

As before,  $\tilde{\mathbf{y}}_{n_r}^{(f)}$  is the permuted version of  $\mathbf{y}_{n_r}^{(f)}$ , so that the vector  $\tilde{\mathbf{y}}_{n_r}^{(f)}$  can be splitted in the pilot vector and the data vector

$$\tilde{\mathbf{y}}_{n_r}^{(f)} = \mathbf{P}^T \mathbf{y}_{n_r}^{(f)} = \left[ \mathbf{y}_{p, n_r}^{(f)T} \mathbf{y}_{d, n_r}^{(f)T} \right]^T. \quad (2.18)$$

Using this notation, Equation (2.10) can be expressed in two equivalent forms

$$\mathbf{y}_{n_r}^{(f)} = \sum_{n_t=1}^{N_t} \mathbf{h}_{n_t, n_r}^{(f)} \odot \mathbf{x}_{n_t}^{(f)} + \mathbf{w}_{n_r}^{(f)} \quad (2.19)$$

$$\tilde{\mathbf{y}}_{n_r}^{(f)} = \sum_{n_t=1}^{N_t} \tilde{\mathbf{h}}_{n_t, n_r}^{(f)} \odot \tilde{\mathbf{x}}_{n_t}^{(f)} + \mathbf{P}^T \mathbf{w}_{n_r}^{(f)} \quad (2.20)$$

where  $\odot$  denotes element wise multiplication of two vectors. From channel estimation point of view the symbol on pilot positions are of most interest. Equation (2.20) on the pilot positions reduces to

$$\mathbf{y}_{p, n_r}^{(f)} = \mathbf{h}_{p, n_t, n_r}^{(f)} \odot \mathbf{x}_{p, n_t}^{(f)} + \mathbf{w}_{p, n_r}^{(f)}. \quad (2.21)$$



The sum in Equation (2.20) disappears because of the following reason. Whenever a pilot is located at the  $n_t$ -th transmit antenna port within the  $n_s$ -th OFDM symbol on the  $k$ -th subcarrier, symbols, at the remaining transmit antenna ports zeros are transmitted on the same positions (for more details see Section 2.2).

## Chapter 3

# Channel Estimation for Block Fading

In the following chapter, I will discuss channel estimation assuming block fading, that is, the coherence time of the channel is long enough that the channel impulse response is approximately constant over the duration of one subframe. According to [3] the duration of one subframe is 1 ms. The coherence time of a channel is in [6] defined as

$$T_c = \frac{1}{4D_s} \quad (3.1)$$

with  $D_s$  being the Doppler spread, that is, the largest difference between the Doppler shifts

$$D_s = \max_{i,j} |f_{s_i} - f_{s_j}| \quad (3.2)$$

where  $f_{s_i}$  is the Doppler shift of the  $i$ -th path. Doppler shift is defined as frequency shift due the relative motion between observation point and fader

$$f_s = f_c \frac{v}{c_0} \quad (3.3)$$

with  $v$  being the relative velocity and  $c_0$  the speed of light. Assuming Jakes model, where  $D_s = 2f_{s,\max}$ , using a realistic carrier frequency (for example  $f_c = 2.11$  GHz), the maximum relative velocity between the receiver and faders has to be smaller than  $v = 17.7$  m/s (I will further investigate this theoretical statement in Chapter 4. )

If the block fading assumption is fulfilled, then the channel will be constant over the duration of one subframe. The elements  $\mathbf{h}_{n_t, n_r, n_s}^{(f)}$  of  $\mathbf{h}_{n_t, n_r}^{(f)}$  from Equation (2.15) are independent of  $n_s$ . Therefore, the output of the block fading estimator will be the estimated channel vector

$$\hat{\mathbf{h}}_{n_t, n_r, n_s} = [\hat{h}_{n_t, n_r, n_s, 0} \cdots \hat{h}_{n_t, n_r, n_s, K_{\text{sub}}-1}]^T \quad (3.4)$$

with the elements  $\hat{h}_{n_t, n_r, n_s, k}$  corresponding to the channel estimate for the  $k$ -th subcarrier between the  $n_t$ -th and  $n_r$ -th antenna port. Although the estimate is independent of  $n_s$ , I won't omit the corresponding index  $n_s$ , because it might cause confusion with the vector  $\mathbf{h}_{n_t, n_r}$ , which length is  $N_s$  times larger than the length of  $\mathbf{h}_{n_t, n_r, n_s}$ . From this point on, all quantities are considered in the frequency domain, therefore I will omit the index (f).

### 3.1 Least Squares Channel Estimation

Whenever there is a pilot on the  $k$ -th subcarrier within the  $n_s$ -th OFDM symbol on the  $n_t$ -th transmit antenna port, the symbols on the same subcarrier within the same OFDM symbol on the remaining transmit antenna ports are 0. This reduces the spectral efficiency, however such a scheme also preserves the orthogonality between the pilot symbols at different transmit antenna ports allowing to estimate a MIMO channel as  $N_t N_r$  independent Single Input Single Output (SISO) channels. (In Section 3.2.2 I will discuss an approach, which estimates a MIMO channel using spatial correlation between channels.) To estimate the channel coefficient on the pilot positions, the first obvious approach is to divide the received symbol on the desired position by the corresponding pilot symbol

$$\hat{h}_{\text{LS}, p, n_t, n_r} = \frac{y_{p, n_r}}{x_{p, n_t}} = h_{p, n_t, n_r} + \frac{z_{p, n_r}}{x_{p, n_t}} \quad (3.5)$$

where subscript p indicates symbol on the pilot positions. This approach corresponds to the Least Squares (LS) channel estimate from [7]. Due to the LTE system design and using Equation (3.5) it is possible to calculate just the channel estimates on the pilot positions, the channel estimate on the remaining positions has to be obtained by interpolation.

At the 1st and the 2nd transmit antenna port within an LTE subframe there are two pilot symbols on every 3rd subcarrier. If the assumption of block fading is fulfilled, then both pilot symbols are transferred over the same channel, that is, the  $h_{p, n_t, n_r}$  for both pilot symbols are exactly the same. The noise term in Equation (3.5) is zero mean, therefore averaging over two channel coefficient estimates will improve the estimate (thereby reducing the noise term of the estimate).

$$\hat{h}_{\text{LS}, n_t, n_r, n_s, k_p} = \frac{1}{2} \left[ \frac{y_{p_1, n_r}}{x_{p_1, n_t}} + \frac{y_{p_2, n_r}}{x_{p_2, n_t}} \right] = h_{n_t, n_r, n_s, k_p} + \frac{1}{2} \left[ \frac{z_{p_1, n_r}}{x_{p_1, n_t}} + \frac{z_{p_2, n_r}}{x_{p_2, n_t}} \right] \quad (3.6)$$

where  $\hat{h}_{\text{LS}, n_t, n_r, n_s, k_p}$  is the LS estimate of the channel coefficient between the  $n_t$ -th and  $n_r$ -th antenna port on the  $k_p$ -th subcarrier (lower index p refers to

subcarriers, on which the pilot symbols are located) and  $p_1$  and  $p_2$  are the pilot positions on the same  $k$ -th subcarrier (they are located within different OFDM symbols).

### Interpolation

Pilot symbols insertion and the LS estimation of the channel on the pilot positions corresponds to the sampling of the channel. To obtain the remaining channel coefficients, interpolation has to be used.

#### Linear Interpolation

Linear interpolation is the easiest way to estimate the channel coefficients on the data positions. Two adjacent channel estimates are connected by the help of a linear function. This linear function is sampled at the missing data positions.

$$\hat{h}_{n_t, n_r, n_s, k_d} = \hat{h}_{n_t, n_r, n_s, k_{p_1}} + (k_d - k_{p_1}) \frac{\hat{h}_{n_t, n_r, n_s, k_{p_2}} - \hat{h}_{n_t, n_r, n_s, k_{p_1}}}{k_{p_2} - k_{p_1}} \quad (3.7)$$

where  $k_{p_1}$  and  $k_{p_2}$  are the indices of adjacent subcarriers on which the pilot symbols are located and  $k_d$  is the index of the subcarriers, on which just the data symbols are located, with  $k_{p_1} < k_d < k_{p_2}$ . To estimate channel coefficients, which are not located between two pilot symbols, that is, the edge channel coefficients, one can use linear extrapolation. Figure 3.1 shows the linear interpolation approach on a channel realization. First, the LS channel estimates are calculated and then adjacent LS channel estimates are connected by a linear function. In Figure 3.1 it seems as if the LS points were not connected by linear function. The reason for this appearance is that the absolute value of the estimated channel is plotted. If the real or imaginary part of the channel estimate is plotted, the connection between the LS estimates would be linear.

#### Cubic Interpolation

The approach in cubic interpolation is similar to the one of the linear interpolation, but instead of using linear function to connect adjacent pilot positions, functions up to the 3rd order are used. The complexity of cubic interpolation is higher than the complexity of linear interpolation.

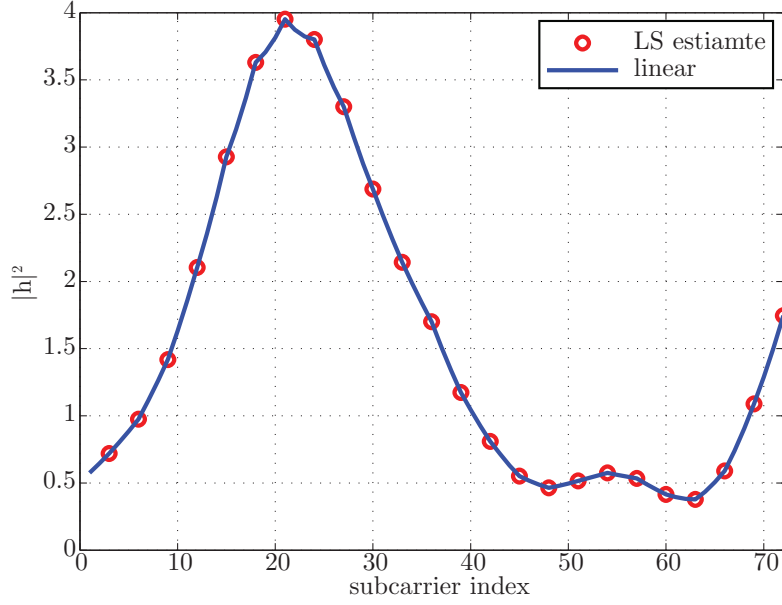


Figure 3.1: Example of linear interpolation

### Spline Interpolation

Spline interpolation uses a low degree polynomial to connect the LS estimates, whereby the continuity is preserved [8].

### Time-Frequency Interpolation

The Time-Frequency (T-F) interpolation uses IFFT/FFT and zero padding. All estimates of the channel  $\hat{h}_{\text{LS},n_t,n_r,k_p}$  are inserted into a length  $K_{\text{sub}}/3$  vector  $\hat{h}_{\text{LS},n_t,n_r}$ . Then the IFFT of the vector  $\hat{h}_{\text{LS},n_t,n_r}$  is performed, to convert the LS channel estimate vector from the frequency to the time domain. After the IFFT, a zero vector of length  $\frac{2}{3}K_{\text{sub}}$  is added. The zero padded vector is a  $K_{\text{sub}}$  length vector. Then the FFT is performed to convert the zero padded vector to the frequency domain. More details on this interpolation technique can be found in [9].

### Sinc Interpolation in the frequency domain

This approach is well known from common signal sampling. Every channel sample (the LS estimate on the subcarriers on which the pilot symbols are located) is multiplied by the sinc function, which has zeros values at the remaining LS estimates the subcarriers on which the pilot symbols are lo-

cated, that is, the sinc function has non zero values on the subcarriers on which just data symbols are located. With the sinc interpolation technique is it possible to recover the original signal perfectly, if two assumption are fulfilled, the Nyquist-Shannon sampling theorem and the signal has to be of infinity length. In practice however, is the length of the signal finite and one can observe edge effect, that is, the channel estimate at the edge shows larger error than elsewhere.

### Sinc Interpolation in the time domain

The previous technique corresponds to the convolution of the sinc function with the LS estimate in the frequency domain. From signal theory it is known, that the convolution in the frequency domain is equivalent to the multiplication in the time domain. The sinc function in the frequency domain corresponds to a rect function in the time domain. With knowledge of those two facts it is possible to perform the interpolation in the time domain, equivalent to the sinc interpolation in the frequency domain. First, the FFT of the LS estimate has to be performed, then the LS estimate in the time domain will be multiplied with the rect function and transformed back to the frequency domain using the FFT.

In Figure 3.2 different interpolation methods are plotted for one channel realization at Signal to Noise Ratio (SNR) = 100 dB. Three facts can be observed:

- Both sinc interpolation techniques are strongly oscillating.
- Especially at low and high subcarrier indices almost all interpolation methods result in different values.
- All interpolation methods except sinc in frequency and time result in similar channel estimates.

All three points will be further investigated in Section 3.4.1.

## 3.2 Linear Minimum Mean Square Error Channel Estimation

The LMMSE channel estimator provides channel coefficients that minimize the mean squared error

$$\epsilon = \mathbb{E} \left\{ \left\| \mathbf{h} - \mathbf{A}_{\text{LMMSE}} \hat{\mathbf{h}}_{\text{LS}} \right\|_2^2 \right\}. \quad (3.8)$$

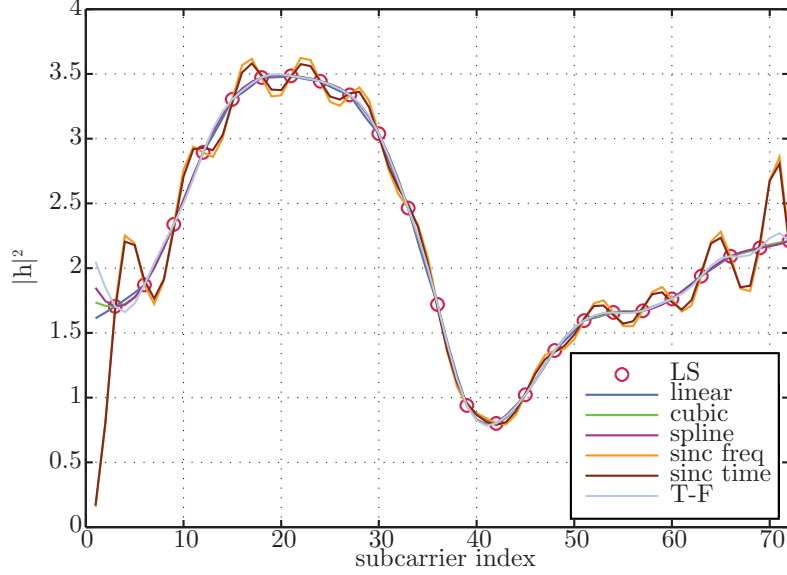


Figure 3.2: Comparison of interpolation techniques for one channel realization

The LMMSE channel estimation can be obtained as filtering of the LS estimate by a matrix  $\mathbf{A}_{\text{LMMSE}}$  [7]

$$\hat{\mathbf{h}}_{\text{LMMSE}} = \mathbf{A}_{\text{LMMSE}} \hat{\mathbf{h}}_{\text{LS}} \quad (3.9)$$

with

$$\mathbf{A}_{\text{LMMSE}} = \mathbf{R}_{\mathbf{h}, \mathbf{h}_{\text{LS}}} (\mathbf{R}_{\mathbf{h}_{\text{LS}}} + \sigma_w^2 \mathbf{I})^{-1}. \quad (3.10)$$

where  $\mathbf{R}_{\mathbf{h}, \mathbf{h}_{\text{LS}}}$  is a crosscorrelation matrix

$$\mathbf{R}_{\mathbf{h}, \mathbf{h}_{\text{LS}}} = \mathbb{E} \{ \mathbf{h} \mathbf{h}_{\text{LS}}^H \} \quad (3.11)$$

and  $\mathbf{R}_{\mathbf{h}_{\text{LS}}}$  is a autocorrelation matrix

$$\mathbf{R}_{\mathbf{h}_{\text{LS}}} = \mathbb{E} \{ \mathbf{h}_{\text{LS}} \mathbf{h}_{\text{LS}}^H \}. \quad (3.12)$$

### 3.2.1 LMMSE Channel Estimation for Spatially Uncorrelated Channels

In the following subsection, I will specialize the LMMSE channel estimator for spatial uncorrelated MIMO channels, which basically consists of  $N_t N_r$

uncorrelated SISO channels. In a real scenario there is almost always spatial correlation between antennas, but if the use of the spatial correlation between the antenna ports is omitted, the computational complexity is reduced. To simplify notation, let  $\hat{\mathbf{h}}_{\text{LS},n_t,n_r,n_s}$  be the vector of the LS estimate between the  $n_t$ -th and  $n_r$ -th antenna on subcarriers with pilot symbol. The length of this vector is  $K_{\text{sub}}/3$  and  $\hat{\mathbf{h}}_{\text{LMMSE},n_t,n_r,n_s}$  is the vector of the permuted LMMSE channel estimate for all subcarriers with length  $K_{\text{sub}}$ . Equation (3.9) and Equation (3.10) can be written as

$$\hat{\mathbf{h}}_{\text{LMMSE},n_t,n_r,n_s} = \mathbf{A}_{\text{LMMSE}} \hat{\mathbf{h}}_{\text{LS},n_t,n_r,n_s} \quad (3.13)$$

and

$$\mathbf{A}_{\text{LMMSE}} = \mathbf{R}_{\tilde{\mathbf{h}}_{n_s}, \mathbf{h}_{\text{LS},n_s}} (\mathbf{R}_{\mathbf{h}_{\text{LS},n_s}} + \sigma_w^2 \mathbf{I})^{-1} \quad (3.14)$$

where

$$\mathbf{R}_{\tilde{\mathbf{h}}_{n_s}, \mathbf{h}_{\text{LS},n_s}} = \mathbb{E} \left\{ \tilde{\mathbf{h}}_{n_t,n_r,n_s} \mathbf{h}_{\text{LS},n_t,n_r,n_s}^H \right\} \quad (3.15)$$

and

$$\mathbf{R}_{\mathbf{h}_{\text{LS},n_s}} = \mathbb{E} \left\{ \mathbf{h}_{\text{LS},n_t,n_r,n_s} \mathbf{h}_{\text{LS},n_t,n_r,n_s}^H \right\}. \quad (3.16)$$

The  $\mathbf{R}_{\tilde{\mathbf{h}}_{n_s}, \mathbf{h}_{\text{LS},n_s}}$  and  $\mathbf{R}_{\mathbf{h}_{\text{LS},n_s}}$  are tall crosscorrelation and square autocorrelation matrices, respectively. To obtain the channel estimate in the correct order, the  $\hat{\mathbf{h}}_{\text{LMMSE},n_t,n_r,n_s}$  has to be multiplied with a  $K_{\text{sub}} \times K_{\text{sub}}$  permutation matrix  $\mathbf{P}$

$$\hat{\mathbf{h}}_{\text{LMMSE},n_t,n_r,n_s} = \mathbf{P} \hat{\mathbf{h}}_{\text{LMMSE},n_t,n_r,n_s} \quad (3.17)$$

### 3.2.2 LMMSE Channel Estimation for Spatially Correlated Channels

If it is possible to estimate spatial correlation between antennas, this knowledge can be used to estimate the channel vector more precise. First, the LS estimate for every SISO channel has to be calculated which will be ordered into the vector  $\mathbf{h}_{\text{LS},n_s}^{(\text{full})}$ . Let  $\tilde{\mathbf{h}}_{n_s}^{(\text{full})}$  be a vector, which is a permuted version of the vector  $\mathbf{h}_{n_s}^{(\text{full})}$  such, that at the beginning of the vector channel coefficients corresponding to the pilot positions of all transmit antennas are located and followed by the remaining channel coefficients (length of this vector is  $K_{\text{sub}}N_tN_r$ ). The vector  $\mathbf{h}_{n_s}^{(\text{full})}$  consists of the channel vectors between all transmit and receive antenna ports.

$$\mathbf{h}_{n_s}^{(\text{full})} = [\mathbf{h}_{0,0,n_s}^T \cdots \mathbf{h}_{N_t-1,N_r-1,n_s}^T]^T. \quad (3.18)$$



Let  $\mathbf{R}_h^{(\text{full})}$  be the autocorrelation matrix of the vector  $\mathbf{h}_{n_s}^{(\text{full})}$ , which has following structure, if the Kronecker model is considered [10]

$$\mathbf{R}_h^{(\text{full})} = \mathbf{R}_T \otimes \mathbf{R}_R \otimes \mathbf{R}_h \quad (3.19)$$

where  $\mathbf{R}_T$  is the spatial autocorrelation matrix between the transmit antennas,  $\mathbf{R}_R$  is the spatial autocorrelation matrix between the receive antennas and  $\mathbf{R}_h$  is the channel autocorrelation matrix. In the following step, the matrix  $\mathbf{R}_h^{(\text{full})}$  has to be permuted, so that the following expression is valid

$$\mathbf{R}_{\tilde{\mathbf{h}}}^{(\text{full})} = \mathbf{P} \mathbf{R}_h^{(\text{full})} \mathbf{P}^T = \mathbb{E} \left\{ \tilde{\mathbf{h}}^{(\text{full})} \tilde{\mathbf{h}}^{(\text{full})H} \right\}. \quad (3.20)$$

To calculate the channel estimate, Equation (3.9) can be used with the following formal changes

$$\hat{\mathbf{h}}_{\text{LMMSE}, n_s}^{(\text{full})} = \mathbf{A}_{\text{LMMSE}}^{(\text{full})} \hat{\mathbf{h}}_{\text{LS}, n_s}^{(\text{full})} \quad (3.21)$$

with

$$\mathbf{A}_{\text{LMMSE}}^{(\text{full})} = \mathbf{R}_{\tilde{\mathbf{h}}_{n_s}^{(\text{full})}, \mathbf{h}_{\text{LS}, n_s}^{(\text{full})}} (\mathbf{R}_{\mathbf{h}_{\text{LS}, n_s}^{(\text{full})}} + \sigma_w^2 \mathbf{I})^{-1} \quad (3.22)$$

where the matrices  $\mathbf{R}_{\tilde{\mathbf{h}}_{n_s}^{(\text{full})}, \mathbf{h}_{\text{LS}, n_s}^{(\text{full})}}$  and  $\mathbf{R}_{\mathbf{h}_{\text{LS}, n_s}^{(\text{full})}}$  are obtained as

$$\mathbf{R}_{\tilde{\mathbf{h}}_{n_s}^{(\text{full})}, \mathbf{h}_{\text{LS}, n_s}^{(\text{full})}} = \left( \mathbf{R}_{\tilde{\mathbf{h}}_{n_s}^{(\text{full})}} \right)_{K_d + K_p, K_p} \quad (3.23)$$

$$\mathbf{R}_{\mathbf{h}_{\text{LS}, n_s}^{(\text{full})}} = \left( \mathbf{R}_{\tilde{\mathbf{h}}_{n_s}^{(\text{full})}} \right)_{K_p, K_p} \quad (3.24)$$

where  $K_d$  is the number of the subcarriers on which just data symbols are located, and  $K_p$  is the number of subcarriers, on which pilot symbols are located. The expression  $(\cdot)_{M, N}$  indicates a submatrix, which is given by the first  $M$  rows and the first  $N$  columns of the matrix.

### 3.3 Approximate LMMSE Channel Estimation

The performance of the LMMSE estimator is in general superb (see Section 3.4.2), but of high computational complexity because of the matrix inversion in Equation (3.10). In a real-time implementation, a reduction of complexity is desired while preserving the performance of the LMMSE estimator. In the following section, I will discuss a low complexity estimator presented in [11], where the authors applied this estimator for Worldwide Interoperability for Microwave Access (WiMAX). The main difference between

LTE and WiMAX from channel estimation point of view is that LTE uses pilot symbols for the channel estimation and WiMAX a preamble [3], [12]. Consequently, the Approximate Linear Minimum Mean Square Error (ALMMSE) presented in [11] has to be adopted for the LTE system.

The two main ideas of the ALMMSE estimator from [11] are:

1. To calculate the LMMSE filtering matrix by using only the correlation between the  $L$  nearest subcarriers instead of using the full correlation between all subcarriers. In case of the LMMSE estimator the correlation with all subcarriers is used. Figure 3.3 depicts the full autocorrelation matrix of dimension  $K_{\text{sub}} \times K_{\text{sub}}$  and its submatrices of dimension  $L \times L$ , which are used by the ALMMSE estimator.
2. To average over all  $L \times L$  matrices to get just one matrix, that approximates the correlation to the  $L$  nearest subcarriers.

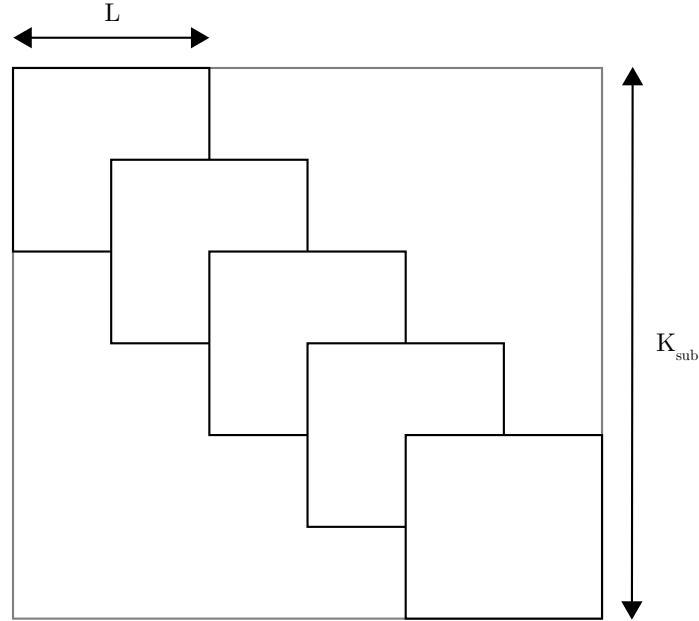


Figure 3.3: Principle of the ALMMSE estimator

Let  $\hat{\mathbf{R}}_{\mathbf{h}}^{(L)}$  be the  $L \times L$  matrix, that approximates the correlation between the  $L$  nearest subcarriers

$$\hat{\mathbf{R}}_{\mathbf{h}}^{(L)} = \frac{1}{\lfloor \frac{K_{\text{sub}}}{L} \rfloor} \sum_{m=0}^{\lfloor \frac{K_{\text{sub}}}{L} \rfloor - 1} (\mathbf{R}_{\mathbf{h}})_{mL+1:(m+1)L, mL+1:(m+1)L} \quad (3.25)$$

where  $(\cdot)_{M:N,M:N}$  denote a submatrix given by the  $M$ -th to  $N$ -th row and the  $M$ -th to  $N$ -th column.

The ALMMSE algorithm for LTE consists of the following steps:

1. Choose  $L$ . The dimension of  $\hat{\mathbf{R}}_{\mathbf{h}}^{(L)}$  is  $L \times L$ .  $L$  is bounded by  $3 \leq L \leq K_{\text{sub}}$ . If  $L = K_{\text{sub}}$  is chosen, the ALMMSE estimator is equal to the LMMSE estimator.
2. Choose the interval of  $L$  consecutive subcarrier indices according to the following rule ( $k$  is the subcarrier index of the channel coefficient to be estimated):

$$\text{Interval} = \begin{cases} [1, L] & ; k \leq \frac{L+1}{2} \\ [k - \lfloor \frac{L-1}{2} \rfloor, k + \lceil \frac{L-1}{2} \rceil] & ; \text{otherwise} \\ [K_{\text{sub}} - L + 1, K_{\text{sub}}] & ; k \geq K_{\text{sub}} - \frac{L-1}{2} \end{cases} \quad (3.26)$$

Let  $\mathbf{h}^{(L)}$  be the channel vector for the subcarriers from the chosen interval.

3. Find the  $K_{\text{p}}^{(L)} = \lfloor \frac{L}{3} \rfloor$  subcarriers on which the pilot symbols are located within the chosen interval. Let  $\mathbf{h}_{\text{p}}^{(L)}$  be the vector of channel coefficients on the pilot symbol positions.
4. Create a permutation matrix  $\mathbf{P}$  of dimension  $L \times L$  with

$$\tilde{\mathbf{h}}^{(L)} = \left[ \mathbf{h}_{\text{p}}^{(L)\text{T}} \mathbf{h}_{\text{d}}^{(L)\text{T}} \right]^{\text{T}} = \mathbf{P}^{\text{T}} \mathbf{h}^{(L)} \quad (3.27)$$

where  $\mathbf{h}_{\text{d}}^{(L)}$  is the channel vector on the data positions within the chosen interval.

5. Permute  $\hat{\mathbf{R}}_{\mathbf{h}}^{(L)}$  with  $\mathbf{P}$

$$\tilde{\mathbf{R}}_{\mathbf{h}}^{(L)} = \mathbf{P}^{\text{T}} \hat{\mathbf{R}}_{\mathbf{h}}^{(L)} \mathbf{P}. \quad (3.28)$$

6. Extract  $\tilde{\mathbf{R}}_{\mathbf{h}_{\text{LS}}}^{(L)}$  and  $\tilde{\mathbf{R}}_{\mathbf{h}, \mathbf{h}_{\text{LS}}}^{(L)}$  from  $\tilde{\mathbf{R}}_{\mathbf{h}_n}^{(L)}$  as

$$\tilde{\mathbf{R}}_{\mathbf{h}_{\text{LS}}}^{(L)} = \left( \tilde{\mathbf{R}}_{\mathbf{h}}^{(L)} \right)_{K_{\text{p}}^{(L)}, K_{\text{p}}^{(L)}} \quad (3.29)$$

$$\tilde{\mathbf{R}}_{\mathbf{h}_n, \mathbf{h}_{\text{LS}, n}}^{(L)} = \left( \tilde{\mathbf{R}}_{\mathbf{h}_n}^{(L)} \right)_{L, K_{\text{p}}^{(L)}}. \quad (3.30)$$

7. Calculate the filtering matrix  $\tilde{\mathbf{F}}^{(L)}$

$$\tilde{\mathbf{F}}^{(L)} = \tilde{\mathbf{R}}_{\mathbf{h}, \mathbf{h}_{\text{LS}}}^{(L)} \left( \tilde{\mathbf{R}}_{\mathbf{h}_{\text{LS}}}^{(L)} + \sigma_w^2 \mathbf{I} \right)^{-1}. \quad (3.31)$$

8. Obtain an estimate of the channel coefficients by multiplying (filtering) the LS estimate on the pilot positions from the chosen interval has to be multiplied (filter) by  $\tilde{\mathbf{F}}^{(L)}$  and permuting (multiplying by  $\mathbf{P}^T$ ). Finally the  $k$ -th element has to selected

$$\mathbf{q} = \mathbf{P}^T \tilde{\mathbf{F}}^{(L)} \tilde{\mathbf{h}}_{\text{LS}}^{(L)} \quad (3.32)$$

$$\hat{h}_{\text{ALMMSE}, k} = \begin{cases} [\mathbf{q}]_k & ; k \leq \frac{L+1}{2} \\ [\mathbf{q}]_{\lceil \frac{L+1}{2} \rceil} & ; \text{otherwise} \\ [\mathbf{q}]_{L+k-K_{\text{sub}}} & ; k \geq K_{\text{sub}} - \frac{L-1}{2} \end{cases} \quad (3.33)$$

$[\mathbf{q}]_k$  means, that the  $k$ -th element of vector  $\mathbf{q}$  will be selected.

### 3.4 Simulation Results

All result are obtained with the LTE Link Level Simulator, developed at the Institute of Communications and Radio-Frequency Engineering (INTHFT), Vienna University of Technology [13]. The simulator is implemented according to [3] in the complex base band. In most cases, I will present a figure of MSE over SNR, which depicts the performance of the estimator and a figure of throughput over SNR, which depicts the influence of the estimator on the performance of the complete system. Table 3.1 presets the most important simulator settings. Those are used for all simulations unless stated differently.

Parameter	Value
Bandwidth	1.4 MHz
Number of transmit antennas	4
Number of receive antennas	2
Transmission mode	Open-loop spatial multiplexing
Channel type	ITU PedB [14]
CQI	9

Table 3.1: Simulator settings for block fading simulations

### 3.4.1 Comparison of Interpolation Techniques

In Figure 3.4 the MSE curves for different interpolation techniques are depicted. The linear interpolator shows the best performance in terms of smallest MSE. This fact is shown also in terms of largest throughput, which is depicted in Figure 3.4. The linear interpolation also has the best performance in terms of throughput among other interpolation techniques and it is also the least complex interpolator from the presented estimators. In Figure 3.5, a saturation behavior of sinc interpolators and of the T-F interpolator can be seen, so the use of them should be limited. Performance of the cubic interpolator is poorer than performance of other interpolators, especially at low SNR values. Therefore, its use should be limited. Pilot symbols are located relative dense on the subcarriers, on every 3rd subcarrier there is at least one pilot symbol, and the adjacent subcarriers are strongly correlated, thus the linear interpolator outperform other interpolators. In Table 3.2 the SNR loss of the individual interpolators is shown. The SNR loss is defined as the difference between the throughput of the considered curves at 90 % of the achievable throughput for the given scenario. There is a gap between the linear interpolator and remaining interpolators.

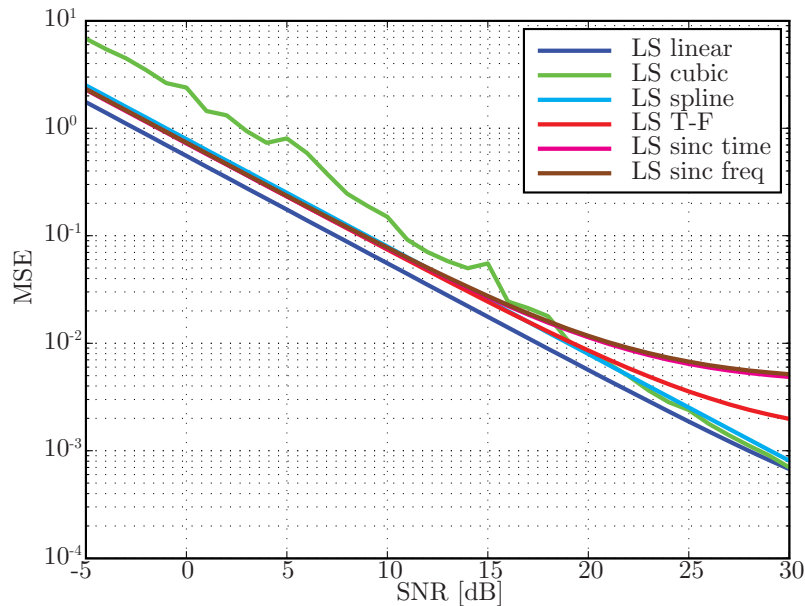


Figure 3.4: MSE for different interpolation techniques

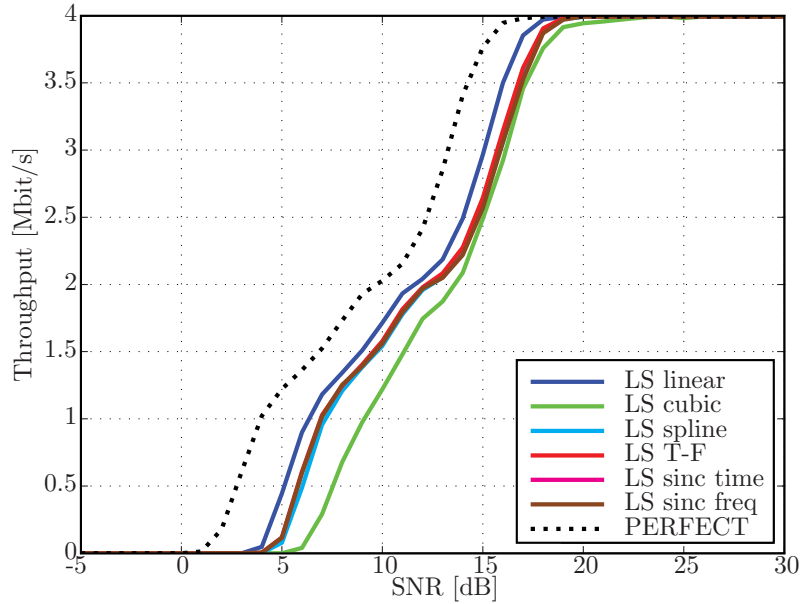


Figure 3.5: Throughput for different interpolation techniques

### Edge effects

Figure 3.2 shows, that the presented interpolation techniques differ mainly in the estimation at the edge of the frequency band. Therefore, I will investigate the performance of the interpolators over subcarrier index. I will present performance of the sinc interpolator, to investigate how significant is the channel estimate error at edge subcarriers. And performance of the linear interpolator, as comparison to the performance of the sinc interpolator. In Figure 3.6 is plotted the MSE over SNR and over subcarrier index for the linear interpolation. It can be seen, that the MSE for high SNR values is close to zero for all subcarriers. For low SNR, an edge effect can be observed, where the MSE is excessively increased. If the linear interpolator is used at low SNR values, one should be aware of this effect.

In Figure 3.7 the MSE over SNR and over subcarrier index is plotted for the sinc interpolation in the frequency domain. At low subcarrier indices, the MSE is larger than at other subcarrier indices. Therefore, the use of sinc interpolation should be always carefully considered. It is surprising, that the the edge effect at low SNR values is more vivid for the linear interpolation than for the sinc interpolation.

Interpolator	SNR loss [dB]
linear	1.7
cubic	2.8
spline	2.5
T-F	2.4
sinc in the frequency domain	2.6
sinc in the time domain	2.6

Table 3.2: SNR loss of different Interpolation techniques to the system with perfect channel knowledge

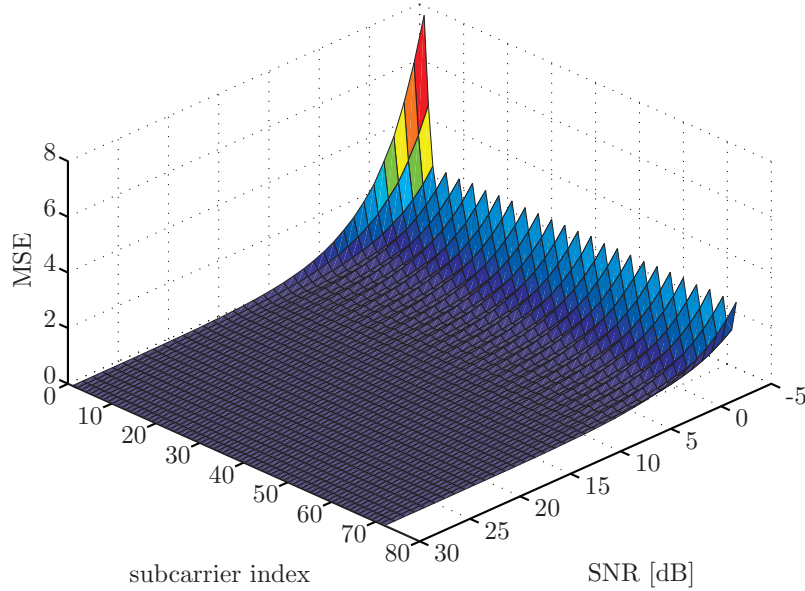


Figure 3.6: MSE for the linear interpolation over subcarrierindex and SNR

### 3.4.2 LMMSE Channel Estimation

In this part, I will compare the performance of the LMMSE estimator with the LS estimator using the linear interpolation. I will also compare the LMMSE estimator which uses the ideal autocorrelation matrix with one that has to estimate the autocorrelation matrix. Finally, I will compare the performance of the LMMSE estimator for spatially correlated channels and the LMMSE for spatially uncorrelated channels applied on a spatially correlated MIMO channel.

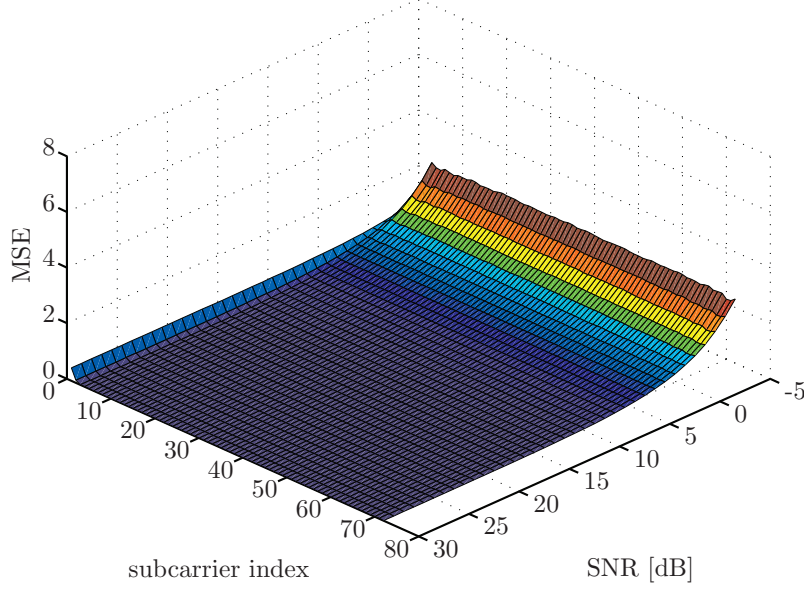


Figure 3.7: MSE for the sinc interpolation in the frequency domain over subcarrierindex and SNR

### LMMSE Channel Estimation versus LS Channel Estimation

In Figure 3.8 and Figure 3.9, the LS estimator is compared to the LMMSE estimator. The performance increase of the LMMSE estimator is obvious. The SNR gain of the LMMSE estimator over the LS estimator is approximately 1.4 dB. In terms of throughput, the system using the LMMSE estimator is approximately 0.5 dB worse than the system with perfect channel knowledge. However, the use of the LMMSE estimator is connected with some problems. The second order statistics of the channel and the noise are necessary, and have therefore to be estimated. In the presented figures, I assumed that the channel statistics and noise power are known perfectly. To calculate the LMMSE filtering matrix, a matrix inverse has to be calculated. In general, matrix inversion is a complex operation, which increases the overall complexity of the estimator.

### Non Ideal Autocorrelation Matrix

In practice, a user does not know the second order statistics of the channel (i.e.  $\mathbf{R}_{h,LS}$  and  $\mathbf{R}_{h,LS}$  from Equation (3.10) are unknown). One possibility to solve this problem, is to save autocorrelation matrices for typical scenarios



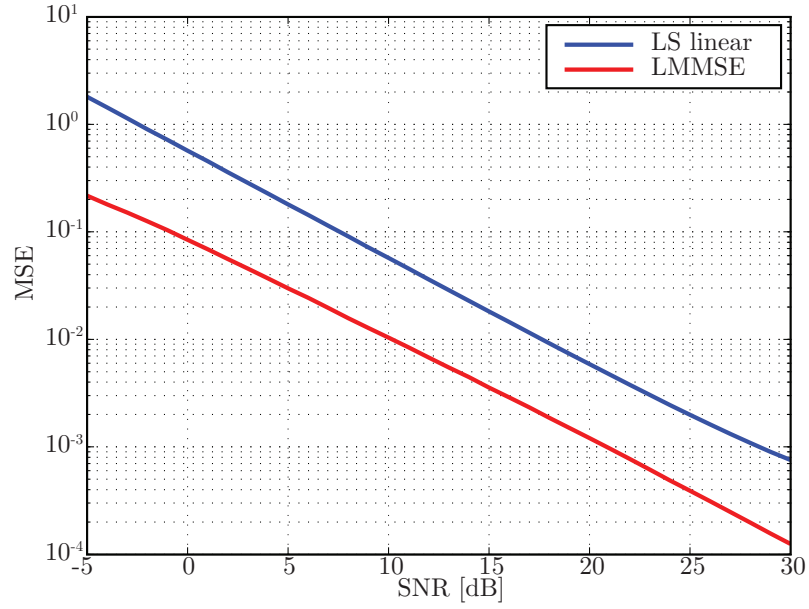


Figure 3.8: MSE for the LMMSE estimator versus the LS estimator

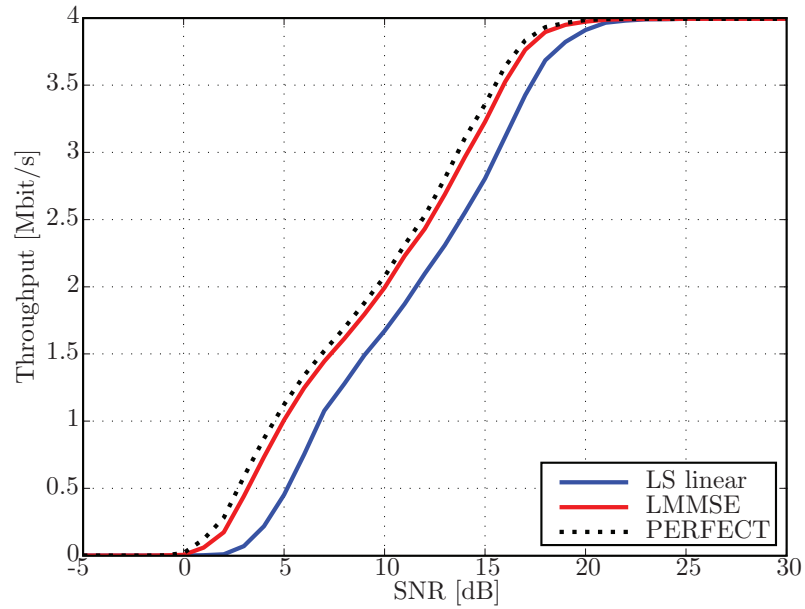


Figure 3.9: Throughput for the LMMSE estimator versus the LS estimator

and let the User Equipment (UE) update it, or let the UE to estimate its own autocorrelation matrix. I implemented the following algorithm to estimate the autocorrelation matrix:

1. The first  $M$  subframes are dedicated just for the estimation of the autocorrelation matrix  $\hat{\mathbf{R}}_{\mathbf{h}}$ .
2. For the first  $M$  subframes, LS estimation with the linear interpolation is performed.
3. The autocorrelation matrix is estimated as

$$\hat{\mathbf{R}}_{\mathbf{h}} = \frac{1}{Mn_t n_r} \sum_{m=0}^{M-1} \sum_{n_t=0}^{n_t-1} \sum_{n_r=0}^{n_r-1} \hat{\mathbf{h}}_{\text{LS},m,n_t,n_r} \hat{\mathbf{h}}_{\text{LS},m,n_t,n_r}^H. \quad (3.34)$$

$M$  should be chosen such, that the matrix  $\hat{\mathbf{R}}_{\mathbf{h}}$  is full rank. In the following simulation, I set  $M = 20$  in a  $4 \times 2$  system, which means that the autocorrelation matrix is estimated over 160 channel realizations ( $MN_t N_r$ ). In Figure 3.10 and Figure 3.11 the performance of systems with the ideal autocorrelation matrix and with the estimated autocorrelation matrix are compared. As expected, the performance of the system with estimated autocorrelation matrix is decreased. However, the performance is much better than the system with LS estimator. The SNR loss of the system with estimated autocorrelation matrix to the system with ideal autocorrelation matrix is approximately 0.5 dB.

Figure 3.12 and Figure 3.13 show the performance of the system using the estimated autocorrelation matrix over  $M$  MIMO channel realizations over which the autocorrelation matrix is calculated. It can be seen, that the MSE saturates for  $M$  larger than 10, which is the condition for full rank. If throughput is considered, the system saturates even before  $M = 10$ . In the simulation, the individual SISO channels of the MIMO channel were assumed uncorrelated. Therefore, if the SISO channels of the MIMO channel were correlated, the performance saturation would occur for  $M > 10$ .

### LMMSE Channel Estimation for Spatially Correlated Channels

In Figure 3.14 and Figure 3.15 the LMMSE estimator for spatially correlated channels, which knows the spatial correlation between the antennas perfectly and the LMMSE estimator, which is not using the spatial correlation for channel estimation are compared. To generate a spatially correlated MIMO channel, the Kronecker model with 0.3 correlation coefficients is used. There

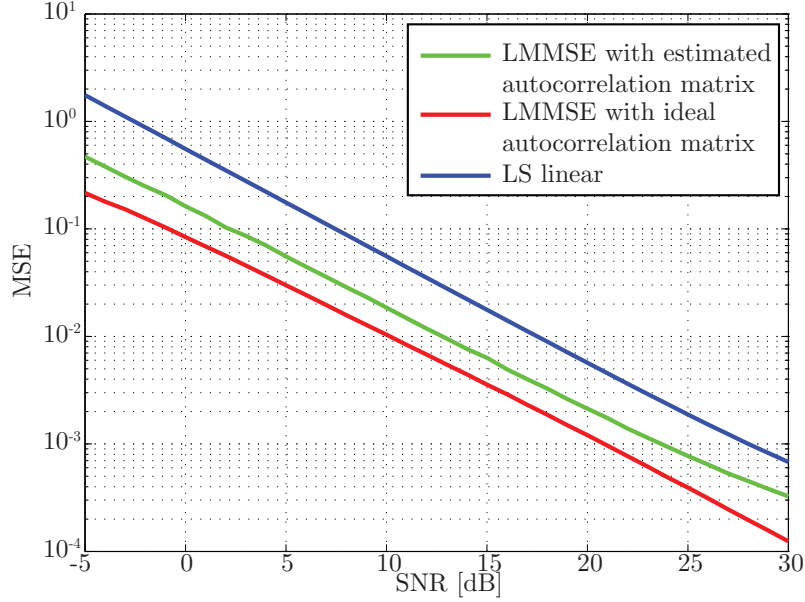


Figure 3.10: MSE for the LMMSE estimator with estimated autocorrelation matrix

is no significant improvement of performance observable. To be able to use the LMMSE estimator for spatial correlated channels, spatial correlation between antennas has to be estimated and the dimension of the matrix to invert is  $N_t N_r$ -times larger than the dimension of matrix to invert in case of the LMMSE estimator, which does not use spatial correlation between antennas. Thus, it does not seem reasonable to utilize the spatial correlation between antennas for channel estimation.

### 3.4.3 ALMMSE Channel Estimation

In this section, I will present results of the ALMMSE channel estimator performance. In Figure 3.16 and Figure 3.17 performance of the ALMMSE estimator with different values of  $L$  is plotted. It can be seen, that with increasing  $L$ , also the MSE is decreasing and throughput is increasing. For  $L = K$  the ALMMSE estimator is equal to the LMMSE estimator. It is obvious, that with increasing  $L$  also the complexity of the estimator is increasing. This fact allows to adjust the performance and complexity of the estimator to achieve a good trade-off.

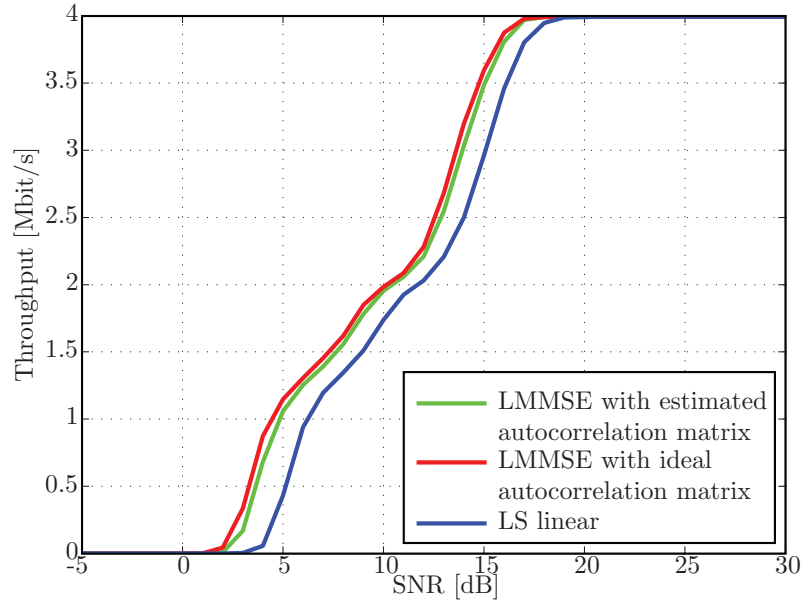


Figure 3.11: Throughput for the LMMSE estimator with estimated autocorrelation matrix

For  $L = 3$  just one channel estimate on a pilot position is used to estimate the channel vector. This approach corresponds to nearest neighbor interpolation, where the estimate on the data position is equal to the estimate on the closest pilot position. Therefore, the performance of the ALMMSE estimator with  $L = 3$  is poorer than the performance of the LS estimator.

In Figure 3.18 the SNR loss of ALMMSE to LMMSE in dependence of chosen  $L$  is plotted. To overcome LS performance,  $L \geq 6$  has to be chosen.

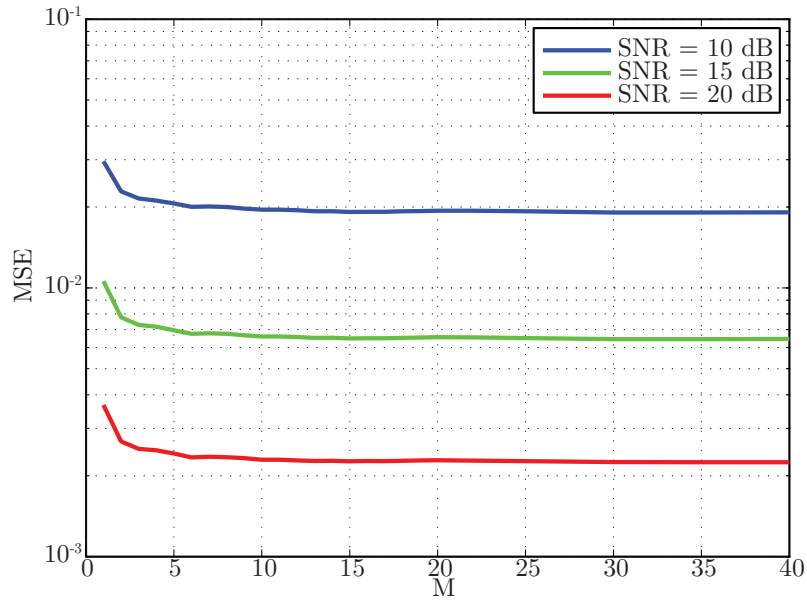


Figure 3.12: MSE for the LMMSE estimator with estimated autocorrelation matrix over  $M$

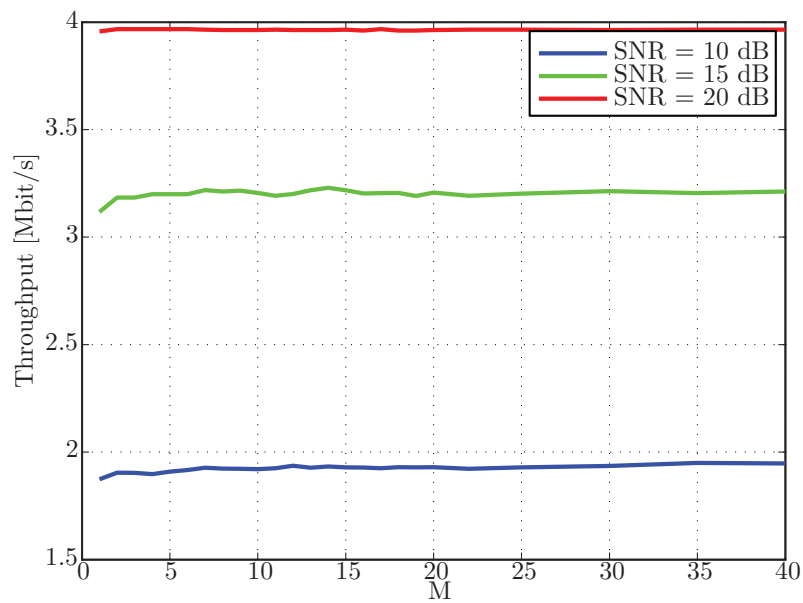


Figure 3.13: Throughput for the LMMSE estimator with estimated autocorrelation matrix over  $M$

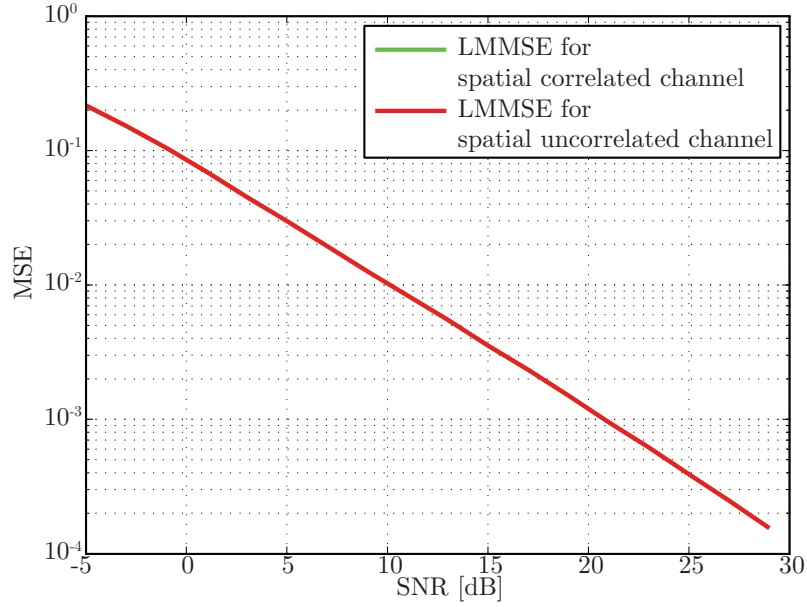


Figure 3.14: MSE for the LMMSE estimator for spatially correlated channels

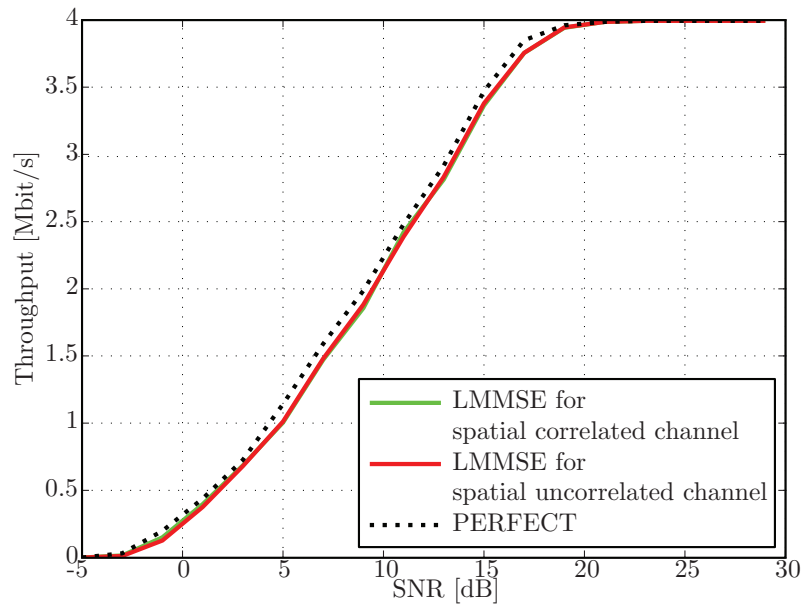
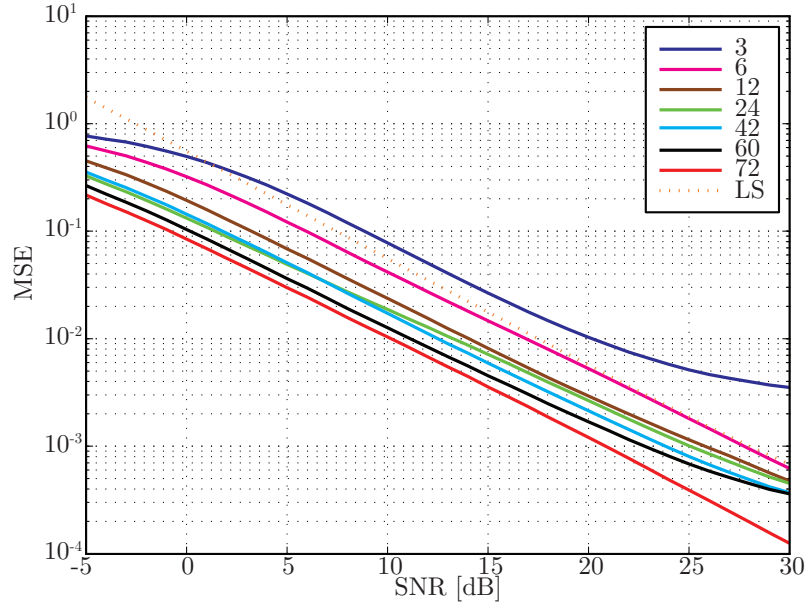
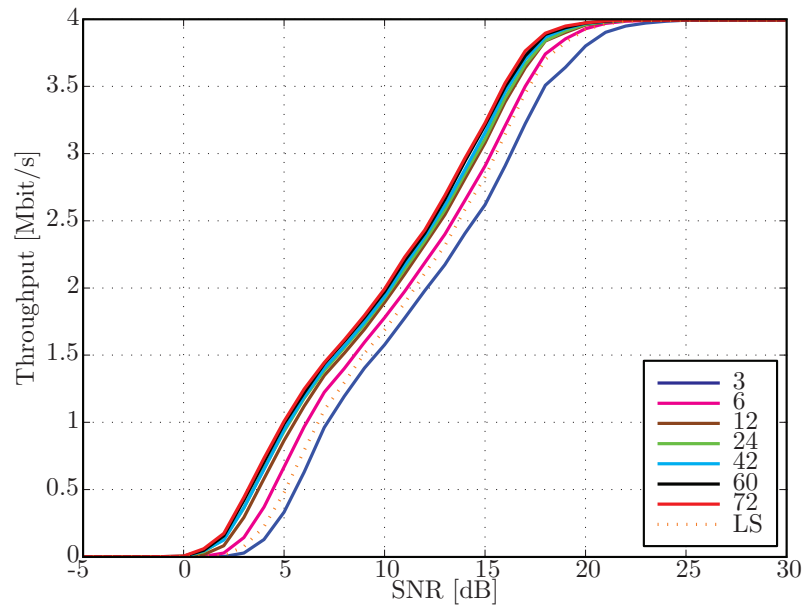


Figure 3.15: Throughput for the LMMSE estimator for spatially correlated channels

Figure 3.16: MSE for the ALMMSE estimator with different  $L$ Figure 3.17: Throughput for the ALMMSE estimator with different  $L$

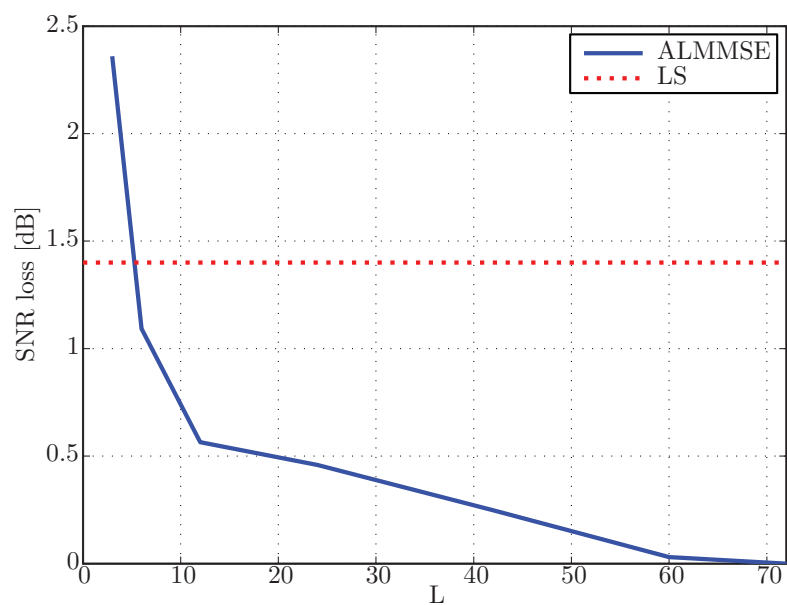


Figure 3.18: SNR loss of the ALMMSE estimator to the LMMSE estimator over L



# Chapter 4

## Channel Estimation for Fast Fading

In the following chapter, I will discuss channel estimation assuming fast fading, that is, the coherence time of the channel is so short that the channel impulse response changes significantly during one subframe. In the used channel model, the maximum Doppler shift frequency  $f_{s,\max}$ , corresponding to the maximum velocity  $v_{\max}$  according to Equation (3.3), can be chosen. Due the vividness of velocity, I will use  $v_{\max}$  to describe the fast fading channel. If  $v_{\max}$  is set to 0, the fast fading channel degrades into a block fading channel. The channel estimation for fast fading is in general more complex than for block fading, therefore it is important for a real-time implementation to decide correctly which type of estimator to use.

The output of the fast fading estimator will be the channel estimate  $\hat{\mathbf{h}}_{n_t, n_r}$  between all transmit and receive antenna ports (this vector has the same structure as  $\mathbf{h}_{n_t, n_r}$  in Equation (2.15)). This vector can be equivalently written as matrix

$$\hat{\mathbf{H}}_{n_t, n_r} = [\hat{\mathbf{h}}_{n_t, n_r, 0}^T \cdots \hat{\mathbf{h}}_{n_t, n_r, N_s - 1}^T] \quad (4.1)$$

where  $\hat{\mathbf{h}}_{n_t, n_r, n_s}$  is the channel estimate vector of the  $n_s$ -th OFDM symbol. The matrix  $\hat{\mathbf{H}}_{n_t, n_r}$  corresponds to the time-frequency grid of a subframe.

### 4.1 Least Square Channel Estimation

As in Section 3.1, the first step toward the LS estimate is to divide the received symbol at a pilot symbol position  $y_{p, n_r}$  at the  $n_r$ -th receive antenna port by the known transmitted pilot symbol  $x_{p, n_t}$  of the  $n_t$ -th transmit an-

tenna port.

$$\hat{h}_{\text{LS},p,n_t,n_r} = \frac{y_{p,n_r}}{x_{p,n_t}} = h_{p,n_t,n_r} + \frac{z_{p,n_r}}{x_{p,n_t}}. \quad (4.2)$$

The pilot symbol positions indicated by  $p$  corresponds to some position within the time-frequency grid. The main difference to Equation (3.6) is, that also the index of OFDM symbol  $n_s$  has to be considered and that in general it is not allowed to average over two channel coefficients on the same subcarrier. Therefore the fast fading LS estimator has poorer performance in case  $v_{\max} = 0$  as the block fading estimator for same scenario. To obtain the missing data channel coefficients, again interpolation has to be performed. The main difference to Section 3.1 is, that instead of 1D interpolation, 2D interpolation has to be used.

### Linear Interpolation

This algorithm solves the so-called triangulation problem (for more details see [15]). For every channel coefficient which is to estimate, it searches for three nearest LS estimates on the pilot positions in the time-frequency grid, and samples plane spanned by those three points.

### Cubic Interpolation

Cubic interpolation works similar to the linear interpolation, but instead of using just planes, it performs triangle-based cubic interpolation [16].

### V4 Interpolation

This algorithm uses method presented in [17]. The complexity is higher than of the linear or cubic interpolation.

## 4.2 Linear Minimum Mean Square Error Channel Estimation

The approach of the LMMSE estimator for fast fading is similar to the LMMSE for block fading. It is based on Equation (3.9). The MIMO channel will be estimated as  $N_t N_r$  independent SISO channels. This estimator can be used also for spatially correlated MIMO channels. Let  $\hat{\mathbf{h}}_{\text{LS},n_t,n_r}$  be the vector of the LS estimate for the SISO channel between the  $n_t$ -th transmit and the  $n_r$ -th receive antenna ports on the pilot positions, with length  $N_p$ , which is

the number of pilot symbols. The autocorrelation matrix  $\mathbf{R}_{\mathbf{h}}$  is given by

$$\mathbf{R}_{\mathbf{h}} = \mathbb{E} \left\{ \mathbf{h}_{n_t, n_r} \mathbf{h}_{n_t, n_r}^H \right\}. \quad (4.3)$$

In contrast to Section 3.2, the vector to estimate in this section is  $N_s$  time longer than the one in Section 3.2, therefore also the dimension of  $\mathbf{R}_{\mathbf{h}}$  is correspondingly larger. The autocorrelation matrix can be written as

$$\mathbf{R}_{\mathbf{h}} = \mathbf{R}_{\text{time}} \otimes \mathbf{R}_{\mathbf{h}_{n_s}} \quad (4.4)$$

where  $\mathbf{R}_{\text{time}}$  is an  $N_s \times N_s$  matrix describing the time correlation between the OFDM symbols and  $\mathbf{R}_{\mathbf{h}_{n_s}}$  is an  $K_{\text{sub}} \times K_{\text{sub}}$  matrix describing the frequency correlation of the subcarriers. The index  $n_s$  in Equation (4.4) does not indicate time dependency, but indicates, that the matrix  $\mathbf{R}_{\mathbf{h}_{n_s}}$  comprises correlation within one OFDM symbol. To obtain the LMMSE channel estimate, the LS channel estimate has to be filtered by a filter matrix  $\mathbf{A}_{\text{LMMSE}}$ , which is in the case of fast fading

$$\mathbf{A}_{\text{LMMSE}} = \mathbf{R}_{\tilde{\mathbf{h}}, \mathbf{h}_{\text{LS}}} (\mathbf{R}_{\mathbf{h}_{\text{LS}}} + \sigma_w^2 \mathbf{I})^{-1}. \quad (4.5)$$

To obtain the matrices  $\mathbf{R}_{\tilde{\mathbf{h}}, \mathbf{h}_{\text{LS}}}$  and  $\mathbf{R}_{\mathbf{h}_{\text{LS}}}$ , which are necessary to calculate the LMMSE filtering matrix, the matrix  $\mathbf{R}_{\mathbf{h}}$  has to be permuted

$$\mathbf{R}_{\tilde{\mathbf{h}}} = \mathbf{P} \mathbf{R}_{\mathbf{h}} \mathbf{P}^T \quad (4.6)$$

and the submatrices have to be chosen

$$\mathbf{R}_{\tilde{\mathbf{h}}, \mathbf{h}_{\text{LS}}} = (\mathbf{R}_{\tilde{\mathbf{h}}})_{N_d + N_p, N_p} \quad (4.7)$$

$$\mathbf{R}_{\mathbf{h}_{\text{LS}}} = (\mathbf{R}_{\tilde{\mathbf{h}}})_{N_p, N_p}. \quad (4.8)$$

The LMMSE channel estimate between the  $n_t$ -th transmit and  $n_r$ -th receive antenna port is obtained as

$$\hat{\tilde{\mathbf{h}}}_{\text{LMMSE}, n_t, n_r} = \mathbf{A}_{\text{LMMSE}} \hat{\mathbf{h}}_{\text{LS}, n_t, n_r} \quad (4.9)$$

which has to be permuted with permutation matrix  $\mathbf{P}$  to obtain the channel estimate in the correct order

$$\hat{\mathbf{h}}_{\text{LMMSE}, n_t, n_r} = \mathbf{P} \hat{\tilde{\mathbf{h}}}_{\text{LMMSE}, n_t, n_r}. \quad (4.10)$$

### 4.3 Approximate LMMSE Channel Estimation

In the following section, I present a novel fast fading channel estimator, which approximates the LMMSE channel estimator. The main idea is to make use of the known structure of the channel autocorrelation matrix, given by Equation (4.4). The standard LMMSE filtering matrix is obtained by minimizing Equation (3.8). Let us consider the following problem

$$\min_{\mathbf{B}_{\text{freq}}, \mathbf{C}_{\text{time}}} \mathbb{E} \left\{ \|\mathbf{H} - \mathbf{B}_{\text{freq}} \hat{\mathbf{H}}_{\text{LS}} \mathbf{C}_{\text{time}}^T\|_F^2 \right\} \quad (4.11)$$

where  $\mathbf{H}$  and  $\hat{\mathbf{H}}_{\text{LS}}$  have the structure given in Equation (4.1). The approach in Equation (4.11) corresponds to separate filtering over time and frequency of the LS estimate. If the frequency correlation is not changing over time and the time correlation is not frequency dependent, then the channel estimate obtained by separate filtering over time and frequency is identical to the LMMSE channel estimate. After applying the  $\text{vec}(\cdot)$  operator (for details see [18]) on Equation (4.11), and using

$$\text{vec}(\mathbf{H}) = \mathbf{h}, \quad (4.12)$$

$$\text{vec}(\hat{\mathbf{H}}_{\text{LS}}) = \hat{\mathbf{h}}_{\text{LS}}, \quad (4.13)$$

and

$$\text{vec}(\mathbf{B}_{\text{freq}} \hat{\mathbf{H}}_{\text{LS}} \mathbf{C}_{\text{time}}^T) = (\mathbf{C}_{\text{time}} \otimes \mathbf{B}_{\text{freq}}) \text{vec}(\hat{\mathbf{H}}_{\text{LS}}), \quad (4.14)$$

the following expression is obtained

$$\min_{\mathbf{B}_{\text{freq}}, \mathbf{C}_{\text{time}}} \mathbb{E} \left\{ \|\mathbf{h} - (\mathbf{C}_{\text{time}} \otimes \mathbf{B}_{\text{freq}}) \hat{\mathbf{h}}_{\text{LS}}\|_2^2 \right\}. \quad (4.15)$$

The problems formulated in Equation (4.11) and Equation (4.15) are equivalent. Comparing Equation (4.15) to Equation (3.8), the LMMSE estimate is obtained as  $\mathbf{A}_{\text{LMMSE}} = \mathbf{C}_{\text{time}} \otimes \mathbf{B}_{\text{freq}}$ . However, not every matrix can be obtained as Kronecker product of two matrices. Thus, the matrix  $\mathbf{A}_{\text{LMMSE}}$  can only be approximated by  $\mathbf{C}_{\text{time}} \otimes \mathbf{B}_{\text{freq}}$

$$\mathbf{A}_{\text{LMMSE}} \approx \mathbf{C}_{\text{time}} \otimes \mathbf{B}_{\text{freq}}. \quad (4.16)$$

Using Equation (4.4), the matrix  $\mathbf{A}_{\text{LMMSE}}$  is given as

$$\mathbf{A}_{\text{LMMSE}} = \mathbf{R}_{\text{time}} \otimes \mathbf{R}_{\mathbf{h}_{n_s}} (\mathbf{R}_{\text{time}} \otimes \mathbf{R}_{\mathbf{h}_{n_s}} + \sigma_w^2 \mathbf{I})^{-1}. \quad (4.17)$$

The symmetric matrices  $\mathbf{R}_{\text{time}}$  and  $\mathbf{R}_{\mathbf{h}_{n_s}}$  can be rewritten using the eigenvalue decomposition as

$$\mathbf{R}_{\text{time}} = \mathbf{U}_{\text{time}} \mathbf{D}_{\text{time}} \mathbf{U}_{\text{time}}^H \quad (4.18)$$

$$\mathbf{R}_{\mathbf{h}_{n_s}} = \mathbf{U}_{\mathbf{h}_{n_s}} \mathbf{D}_{\mathbf{h}_{n_s}} \mathbf{U}_{\mathbf{h}_{n_s}}^H \quad (4.19)$$

where  $\mathbf{D}_{\text{time}}$  and  $\mathbf{D}_{\mathbf{h}_{n_s}}$  are diagonal matrices, with their corresponding eigenvalues ordered from largest to smallest on the main diagonal.  $\mathbf{U}_{\text{time}}$  and  $\mathbf{U}_{\mathbf{h}_{n_s}}$  are unitary matrices comprising the eigenvectors of the given matrices. The Kronecker product of two matrices has eigenvectors that are given as Kronecker product of the eigenvectors of the matrices, and the eigenvalues are obtained by all possible multiplications of the eigenvalues of the given matrices, thus

$$\mathbf{R}_{\text{time}} \otimes \mathbf{R}_{\mathbf{h}_{n_s}} = (\mathbf{U}_{\text{time}} \otimes \mathbf{U}_{\mathbf{h}_n}) \mathbf{D}_{\mathbf{h}} (\mathbf{U}_{\text{time}} \otimes \mathbf{U}_{\mathbf{h}_n})^H \quad (4.20)$$

where  $\mathbf{D}_{\mathbf{h}}$  is a diagonal matrix with eigenvalues of matrix  $\mathbf{R}_{\text{time}} \otimes \mathbf{R}_{\mathbf{h}_{n_s}}$ , equivalently the matrix  $\mathbf{D}_{\mathbf{h}}$  is given by  $\mathbf{D}_{\text{time}} \otimes \mathbf{D}_{\mathbf{h}_{n_s}}$ . Inserting Equation (4.20) into Equation (4.17) the following expression is obtained

$$\begin{aligned} \mathbf{A}_{\text{LMMSE}} &= (\mathbf{U}_{\text{time}} \otimes \mathbf{U}_{\mathbf{h}_n}) \mathbf{D}_{\mathbf{h}} (\mathbf{U}_{\text{time}} \otimes \mathbf{U}_{\mathbf{h}_n})^H \cdot \\ &\quad \cdot \left( (\mathbf{U}_{\text{time}} \otimes \mathbf{U}_{\mathbf{h}_n}) \mathbf{D}_{\mathbf{h}} (\mathbf{U}_{\text{time}} \otimes \mathbf{U}_{\mathbf{h}_n})^H + \sigma_w^2 \mathbf{I} \right)^{-1}. \end{aligned} \quad (4.21)$$

As a matter of fact, the Kronecker product of two unitary matrices is again a unitary matrix, and therefore

$$\mathbf{I} = (\mathbf{U}_{\text{time}} \otimes \mathbf{U}_{\mathbf{h}_n}) (\mathbf{U}_{\text{time}} \otimes \mathbf{U}_{\mathbf{h}_n})^H. \quad (4.22)$$

Using Equation (4.22), Equation (4.21) can be rewritten as

$$\begin{aligned} \mathbf{A}_{\text{LMMSE}} &= (\mathbf{U}_{\text{time}} \otimes \mathbf{U}_{\mathbf{h}_n}) \mathbf{D}_{\mathbf{h}} (\mathbf{U}_{\text{time}} \otimes \mathbf{U}_{\mathbf{h}_n})^H \cdot \\ &\quad \cdot \left( (\mathbf{U}_{\text{time}} \otimes \mathbf{U}_{\mathbf{h}_n}) (\mathbf{D}_{\mathbf{h}} + \sigma_w^2 \mathbf{I}) (\mathbf{U}_{\text{time}} \otimes \mathbf{U}_{\mathbf{h}_n})^H \right)^{-1}. \end{aligned} \quad (4.23)$$

To calculate the inverse of a matrix, using the eigenvalue decomposition, the following expression holds

$$(\mathbf{U} \mathbf{D} \mathbf{U}^H)^{-1} = \mathbf{U} \mathbf{D}^{-1} \mathbf{U}^H \quad (4.24)$$

thus Equation (4.23) can be equivalently rewritten as

$$\begin{aligned} \mathbf{A}_{\text{LMMSE}} &= (\mathbf{U}_{\text{time}} \otimes \mathbf{U}_{\mathbf{h}_n}) \mathbf{D}_{\mathbf{h}} (\mathbf{U}_{\text{time}} \otimes \mathbf{U}_{\mathbf{h}_n})^H \cdot \\ &\quad \cdot (\mathbf{U}_{\text{time}} \otimes \mathbf{U}_{\mathbf{h}_n}) (\mathbf{D}_{\mathbf{h}} + \sigma_w^2 \mathbf{I})^{-1} (\mathbf{U}_{\text{time}} \otimes \mathbf{U}_{\mathbf{h}_n})^H. \end{aligned} \quad (4.25)$$

Using Equation (4.22), Equation (4.25) can be equivalently rewritten as

$$\mathbf{A}_{\text{LMMSE}} = (\mathbf{U}_{\text{time}} \otimes \mathbf{U}_{\mathbf{h}_n}) \mathbf{D}_{\mathbf{h}} (\mathbf{D}_{\mathbf{h}} + \sigma_w^2 \mathbf{I})^{-1} (\mathbf{U}_{\text{time}} \otimes \mathbf{U}_{\mathbf{h}_n})^H. \quad (4.26)$$

The first assumption towards finding  $\mathbf{B}_{\text{freq}}$  and  $\mathbf{C}_{\text{time}}$ , is that the matrix  $\mathbf{B}_{\text{freq}}$  has the same eigenvectors as the matrix  $\mathbf{R}_{\mathbf{h}_{ns}}$ , and  $\mathbf{C}_{\text{time}}$  as  $\mathbf{R}_{\text{time}}$ . Thus, Equation (4.16) can be written as

$$\mathbf{A}_{\text{LMMSE}} = \mathbf{U}_{\mathbf{h}} \mathbf{D}_{\mathbf{h}} (\mathbf{D}_{\mathbf{h}} + \sigma_w^2 \mathbf{I})^{-1} \mathbf{U}_{\mathbf{h}}^H \approx \mathbf{U}_{\mathbf{h}} \mathbf{D}_{\mathbf{C}_{\text{time}} \otimes \mathbf{B}_{\text{freq}}} \mathbf{U}_{\mathbf{h}}^H \quad (4.27)$$

with  $\mathbf{U}_{\mathbf{h}} = \mathbf{U}_{\text{time}} \otimes \mathbf{U}_{\mathbf{h}_{ns}}$  and  $\mathbf{D}_{\mathbf{C}_{\text{time}} \otimes \mathbf{B}_{\text{freq}}}$  being a diagonal matrix comprising the eigenvalues of the matrix  $\mathbf{C}_{\text{time}} \otimes \mathbf{B}_{\text{freq}}$ , which are given as all possible multiplications of eigenvalues of the matrices  $\mathbf{C}_{\text{time}}$  and  $\mathbf{B}_{\text{freq}}$ . By multiplying the expression in Equation (4.27) by  $\mathbf{U}_{\mathbf{h}}^H$  from the left side and by  $\mathbf{U}_{\mathbf{h}}$  from the right side, the following expression is obtained

$$\mathbf{D}_{\mathbf{h}} (\mathbf{D}_{\mathbf{h}} + \sigma_w^2 \mathbf{I})^{-1} \approx \mathbf{D}_{\mathbf{C}_{\text{time}} \otimes \mathbf{B}_{\text{freq}}}. \quad (4.28)$$

Let  $\underline{\lambda}_{\text{time}}$ ,  $\underline{\lambda}_{\mathbf{h}_{ns}}$ ,  $\underline{\lambda}_{\mathbf{C}_{\text{time}}}$  and  $\underline{\lambda}_{\mathbf{B}_{\text{freq}}}$  denote vectors with eigenvalues of  $\mathbf{R}_{\text{time}}$ ,  $\mathbf{R}_{\mathbf{h}_n}$ ,  $\mathbf{C}_{\text{time}}$  and  $\mathbf{B}_{\text{freq}}$ , respectively. By multiplying  $\underline{\lambda}_{\text{time}}$  with  $\underline{\lambda}_{\mathbf{h}_{ns}}^T$ , a matrix is obtained that comprises all possible multiplications of the elements of the vectors, and thus the eigenvalues of the matrix  $\mathbf{R}_{\text{time}} \otimes \mathbf{R}_{\mathbf{h}_{ns}}$ . To solve Equation (4.28), the eigenvalues of the matrix  $\mathbf{C}_{\text{time}} \otimes \mathbf{B}_{\text{freq}}$  have to be found. The eigenvalues of the matrix  $\mathbf{C}_{\text{time}} \otimes \mathbf{B}_{\text{freq}}$  are given as all possible multiplications of the eigenvalues of the matrices  $\mathbf{C}_{\text{time}}$  and  $\mathbf{B}_{\text{freq}}$ . Thus, the matrix  $\underline{\lambda}_{\mathbf{C}_{\text{time}}} \underline{\lambda}_{\mathbf{B}_{\text{freq}}}^T$  comprises the eigenvalues of the matrix  $\mathbf{C}_{\text{time}} \otimes \mathbf{B}_{\text{freq}}$ . Using matrices  $\underline{\lambda}_{\text{time}} \underline{\lambda}_{\mathbf{h}_{ns}}^T$  and  $\underline{\lambda}_{\mathbf{C}_{\text{time}}} \underline{\lambda}_{\mathbf{B}_{\text{freq}}}^T$ , instead of solving Equation (4.28), the problem can be reformulated as

$$\underline{\lambda}_{\text{time}} \underline{\lambda}_{\mathbf{h}_{ns}}^T ./ (\underline{\lambda}_{\text{time}} \underline{\lambda}_{\mathbf{h}_{ns}}^T + \sigma_w^2 \mathbf{1} \mathbf{1}^T) \approx \underline{\lambda}_{\mathbf{C}_{\text{time}}} \underline{\lambda}_{\mathbf{B}_{\text{freq}}}^T \quad (4.29)$$

where  $\mathbf{1}$  is the all ones vector and  $./$  denotes element-wise division. Equation (4.29) and Equation (4.28) are equivalent. The approximation from Equation (4.29) is a so-called rank one approximation. The best rank one approximation can be found by using a singular value decomposition of the matrix, that has to be approximated

$$\underline{\lambda}_{\text{time}} \underline{\lambda}_{\mathbf{h}_{ns}}^T ./ (\underline{\lambda}_{\text{time}} \underline{\lambda}_{\mathbf{h}_{ns}}^T + \sigma_w^2 \mathbf{1} \mathbf{1}^T) = \mathbf{U} \Sigma \mathbf{V}^H. \quad (4.30)$$

The rank one approximate vectors are then given by the columns of  $\mathbf{U}$  and  $\mathbf{V}$  corresponding to the largest singular value. One of them has to be multiplied by the largest singular value

$$\underline{\lambda}_{\mathbf{C}_{\text{time}}} = \sigma_{\max} \mathbf{u}_{\max}, \quad (4.31)$$

$$\underline{\lambda}_{\mathbf{B}_{\text{freq}}} = \mathbf{v}_{\text{max}}. \quad (4.32)$$

In order to reduce the complexity of the estimator, only  $N_{\text{time}}$  and  $N_{\text{freq}}$  largest eigenvalues of the matrices  $\mathbf{R}_{\text{time}}$  and  $\mathbf{R}_{\mathbf{h}_{n_s}}$  and corresponding eigenvectors are considered.

The presented channel estimation approach is summarized as

$$\hat{\mathbf{H}}_{\text{ALMMSE}} = \mathbf{B}_{\text{freq}} \hat{\mathbf{H}}_{\text{LS}} \mathbf{C}_{\text{time}}^T, \quad (4.33)$$

where the matrices  $\mathbf{B}_{\text{freq}}$  and  $\mathbf{C}_{\text{time}}$  are given by

$$\mathbf{B}_{\text{freq}} = (\mathbf{U}_{\mathbf{h}_n})_{1:N_{\text{freq}}} \text{diag}(\mathbf{v}_{\text{max}}) (\mathbf{U}_{\mathbf{h}_n})_{1:N_{\text{freq}}}^H \quad (4.34)$$

$$\mathbf{C}_{\text{time}} = (\mathbf{U}_{\text{time}})_{1:N_{\text{time}}} \sigma_{\text{max}} \text{diag}(\mathbf{u}_{\text{max}}) (\mathbf{U}_{\text{time}})_{1:N_{\text{time}}}^H \quad (4.35)$$

where  $\text{diag}(\cdot)$  creates a diagonal matrix, and  $(\cdot)_{1:N}$  creates a matrix, which consists of the first  $N$  columns of the matrix. The vectors  $\mathbf{v}_{\text{max}}$  and  $\sigma_{\text{max}} \mathbf{u}_{\text{max}}$  are obtained with help of Equation (4.30), with the vectors  $\underline{\lambda}_{\mathbf{h}_n}$  and  $\underline{\lambda}_{\text{time}}$  being of length  $N_{\text{freq}}$  and  $N_{\text{time}}$ , respectively.

## 4.4 Simulation Results

In the following section, I will discuss the performance of the presented channel estimation technique for fast fading. Furthermore, I will discuss scenarios in which a block fading estimator is applied on a fast fading channel. Additionally, I will discuss the ICI issue. For the following simulations, I used settings of the simulator presented in Table 4.1. In will present simulation results just for  $v_{\text{max}} = 60$  km/h.

Parameter	Value
Bandwidth	1.4 MHz
Number of transmit antennas	4
Number of receive antennas	2
Transmission mode	Open-loop spatial multiplexing
Channel type	ITU VehA [14]
$v_{\text{max}}$	60 km/h
CQI	9

Table 4.1: Simulator settings for fast fading simulations

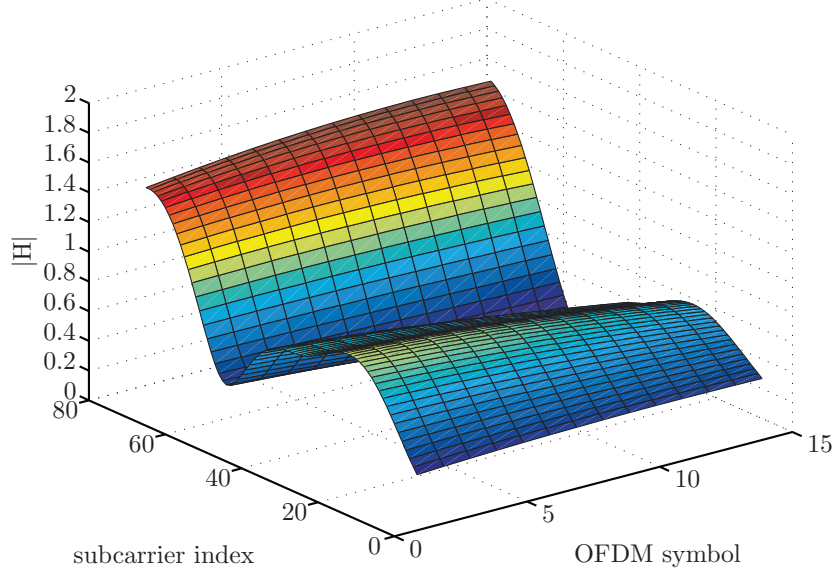


Figure 4.1: Example of a fast fading channel

To obtain a time correlated channel, I used the modified Rosa Zheng model, which is based on [19] and with some modification in the appendix of [20]. In Figure 4.1, an example of a fast fading channel for  $v_{\max} = 60\text{km/h}$  is plotted. The variation of the channel does not look enormous, but I will later present results, which show, that the chosen  $v_{\max}$  corresponds to a fast fading channel. Fast fading implementation in the LTE link level simulator generate a channel impulse response for every sample of the transmit signal in the time domain. This approach corresponds to a real fast fading scenario more than the widely used scenario, where the channel impulse response is assumed to be constant over the duration of one OFDM symbol.

#### 4.4.1 Comparison of Fast Fading Channel Estimation

In Figure 4.2 and Figure 4.3 the MSE and throughput for the LS estimator with different interpolation techniques and also for the LMMSE estimator are plotted. The performance of different interpolation techniques is similar. Therefore, it make sense to use the less complex interpolator, which is the linear interpolator. The SNR loss of a system using the LS estimator with linear interpolation to the system with perfect channel knowledge is approximately 2.3 dB. The system using the LMMSE estimator is loosing around



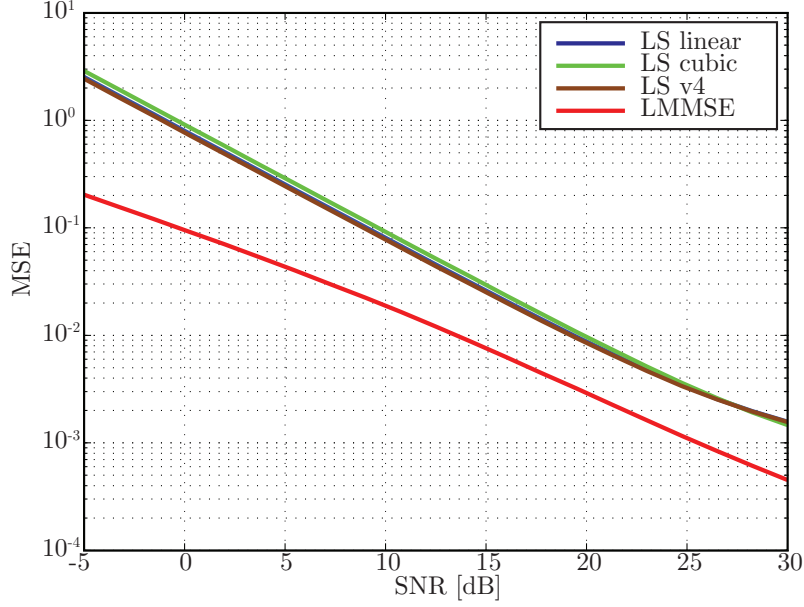


Figure 4.2: MSE for different fast fading estimators

0.8 dB. The SNR loss of the fast fading estimators is slightly larger than the SNR loss of the block fading estimator.

If Figure 4.3 and Figure 3.9 are compared, it is evident that for fast fading scenario with  $v_{\max} = 60\text{km/h}$  the achievable throughput is smaller than for block fading scenario. The reason for this behavior is ICI.

### Robustness against Wrong Temporal Statistics

To calculate the LMMSE filtering matrix, correlation over time is necessary. In Figure 4.2 and Figure 4.3, I assumed that the time correlation between the OFDM symbols of a subframe is perfectly known. Assuming Jakes model, the time correlation is given by the zero-order Bessel function. In practice however, the time correlation has to be estimated. I was not considering estimation of time correlation, but I investigated the robustness of the LMMSE estimator against wrong temporal statistics. In this experiment, the channel is generated using some  $v_{\max}$  and the LMMSE estimator is using  $v_{\text{estimated}}$ , which might be different. In Figure 4.4 and Figure 4.5 the MSE and throughput for a system using the LMMSE estimator, which is using wrong temporal statistics for the channel estimation are shown. The abscissa shows the relative error of the used  $v_{\text{estimated}}$  compared to  $v_{\max}$ . It can be seen, that the

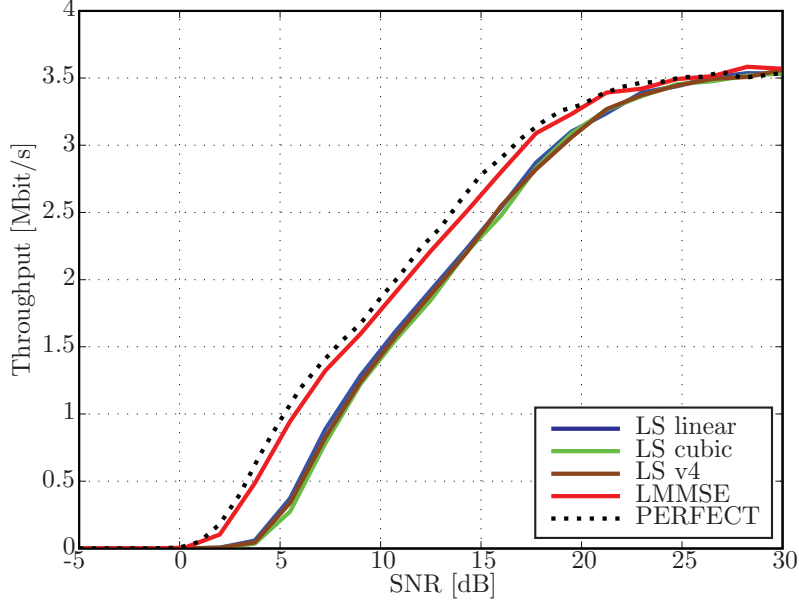


Figure 4.3: Throughput for different fast fading estimators

relative error of the  $v_{\text{estimated}}$  has to be larger than 40 % to see degradation of the performance of the whole system. In Figure 4.4 can be seen, that the MSE is larger in case, when the  $v_{\text{estimated}}$  is smaller than  $v_{\text{max}}$ , than if the used  $v_{\text{estimated}}$  is larger than the true  $v_{\text{max}}$ . Furthermore, it can be seen, that the MSE is not changing significantly if the  $v_{\text{estimated}}$  is in range of  $v_{\text{max}} \pm 20\%$ .

#### 4.4.2 Block Fading Channel Estimation

In this section, I investigate the performance of a system using a block fading estimator in the fast fading scenario. Furthermore, I try to determine  $v_{\text{max}}$ , for which from channel estimation point of view, block fading can be assumed. Finally, I discuss the reasons for the performance degradation in fast fading scenario.

The block fading estimator tries to find a channel estimate, which corresponds to the mean of the channel over the duration of one subframe. If the channel is changing rapidly, the performance of the system will decrease. In Figure 4.6 and Figure 4.7 the MSE and throughput of the system with a block fading estimator applied on fast fading scenario over  $v_{\text{max}}$  are shown. As expected, with increasing  $v_{\text{max}}$  the performance of the overall system is

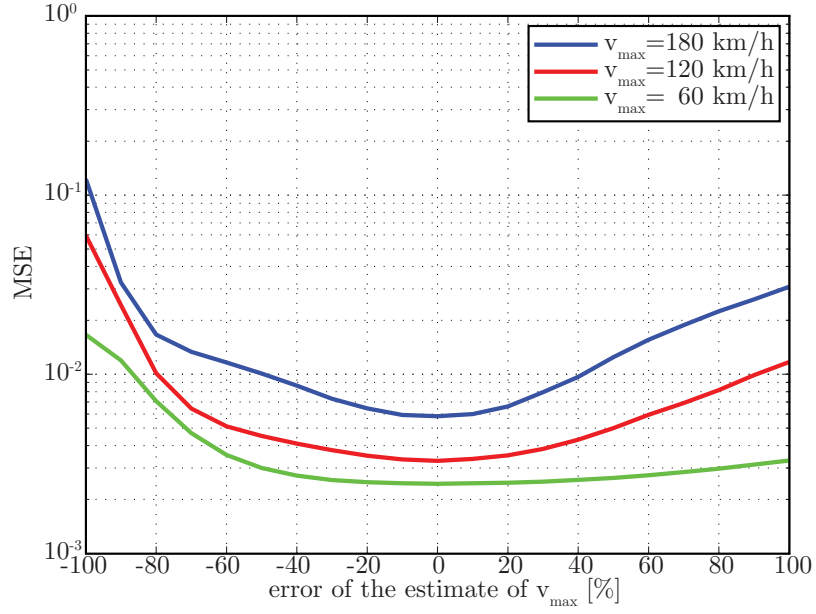


Figure 4.4: MSE for the LMMSE estimator using wrong temporal statistics

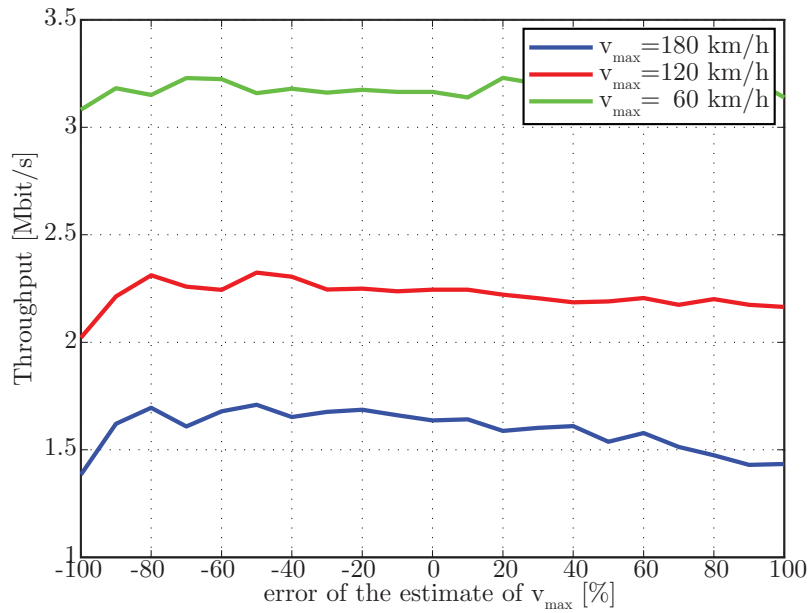


Figure 4.5: Throughput for the LMMSE estimator using wrong temporal statistics

decreasing. The curves for given SNR in Figure 4.7 are not decreasing significantly up to  $v_{\max} = 20$  km/h. Therefore, the block fading assumption is fulfilled for the LTE system, if the  $v_{\max} \leq 20$  km/h is satisfied. This is less than predicted in beginning of Chapter 3.

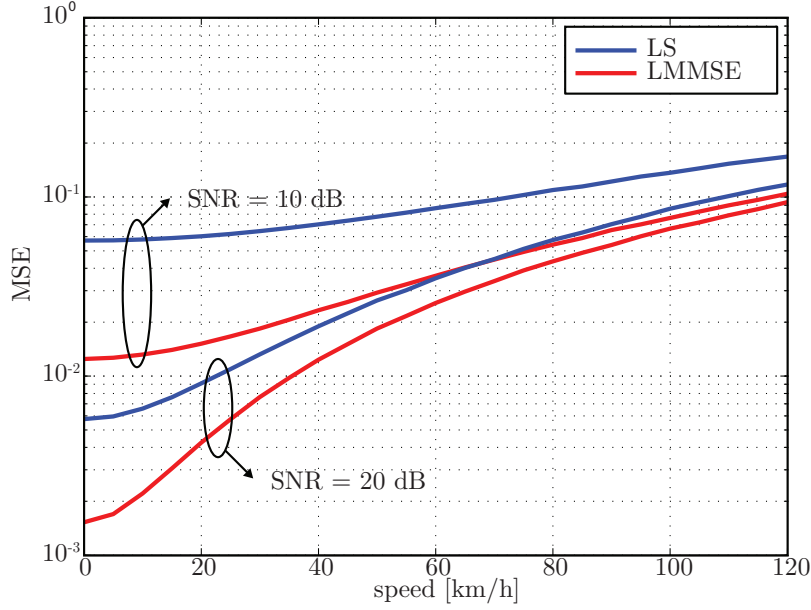


Figure 4.6: MSE for block fading estimator applied on fast fading scenario

In Figure 4.7, it can be seen, that the performance of the system with perfect channel knowledge is also decreasing significantly with  $v_{\max}$ . As it has been shown in Section 4.4.1, the performance of the LMMSE estimator is just slightly poorer than that of a system with perfect channel knowledge. Therefore, there is gain of about 0.25 Mbit/s for  $v_{\max} = 120$  km/h, if a fast fading estimator is used. However, even the performance of a system with perfect channel knowledge is rapidly decreasing with increasing  $v_{\max}$ .

In case of fast fading, the columns of the channel matrix in the time domain  $\mathbf{H}_{n_t, n_r, n_s}^{(t)}$  are time dependent. The matrix  $\mathbf{H}_{n_t, n_r, n_s}^{(t)}$  is not a circulant matrix after multiplication by  $\mathbf{F}_{\text{CP, rem}}$  from left and by  $\mathbf{F}_{\text{CP}}$  from right. Therefore, the channel matrix in the frequency domain  $\mathbf{\Lambda}_{n_t, n_r, n_s}^{(f)}$  is not diagonal. The ICI is caused by the nondiagonal elements of the matrix  $\mathbf{\Lambda}_{n_t, n_r, n_s}^{(f)}$ . Figure 4.8

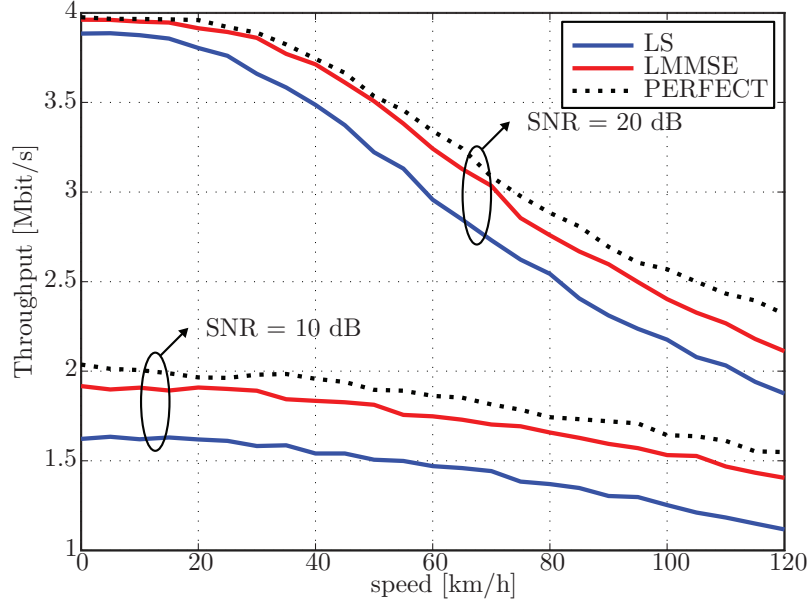


Figure 4.7: Throughput for block fading estimator applied on fast fading scenario

depicts the ICI power over  $v_{\max}$ . The ICI power is defined as

$$P_{\text{ICI}} = \sum_{n_t=1}^{N_t} \mathbb{E} \left\{ \|(\mathbf{\Lambda}_{n_t, n_r, n_s} - \text{diag}(\mathbf{\Lambda}_{n_t, n_r, n_s})) \mathbf{x}_{n_t, n_s}\|_2^2 \right\} \quad (4.36)$$

where the expression  $\text{diag}(\cdot)$  creates a diagonal matrix. For low  $v_{\max}$ , the ICI power is low and the subcarriers are orthogonal. With increasing  $v_{\max}$  also the ICI power is increasing and the orthogonality between the subcarriers is not preserved. Therefore, not just the noise is the limiting factor of the system, but also the interference (e.g. for  $v_{\max} = 120\text{km/h}$ , the Signal to Interference Ratio (SIR) = 10 dB. Therefore, even without any noise, the performance of the system is strongly limited). Consequently, the Signal to Interference and Noise Ratio (SINR) should be considered instead of SNR in fast fading scenarios. Figure 4.9 depicts the SINR mapping for two values of SNR, which shows the influence of the ICI. In a MIMO system, the ICI is caused by signals from more transmit antennas and therefore the ICI in MIMO systems is accentuated (for detailed ICI analysis see [21] and [22]).

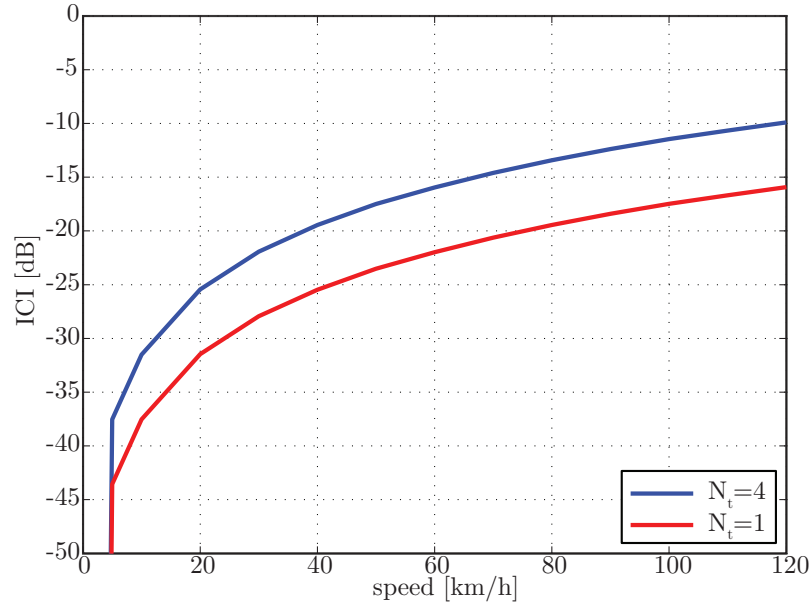


Figure 4.8: Inter carrier interference power

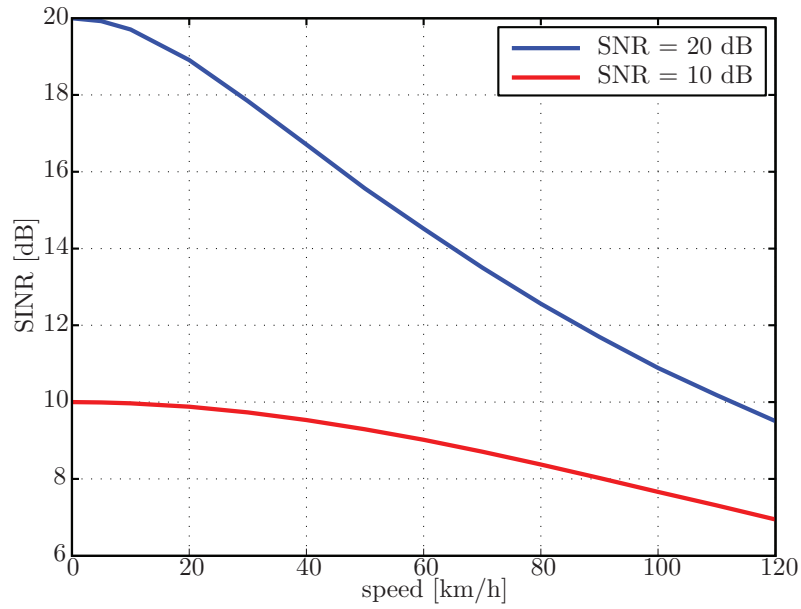


Figure 4.9: SNR/SINR mapping for a moving UE

### 4.4.3 ALMMSE Channel Estimation

In Figure 4.10 and Figure 4.11 performance curves for the ALMMSE channel estimator are plotted, which was presented in Section 4.3. In terms of throughput the ALMMSE estimator is losing 0.1 dB to the LMMSE estimator.

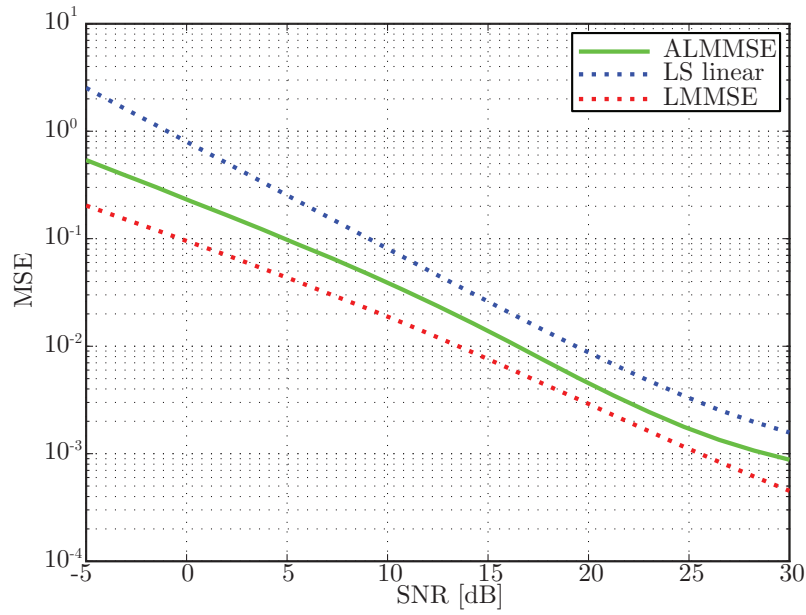


Figure 4.10: MSE for the ALMMSE estimator

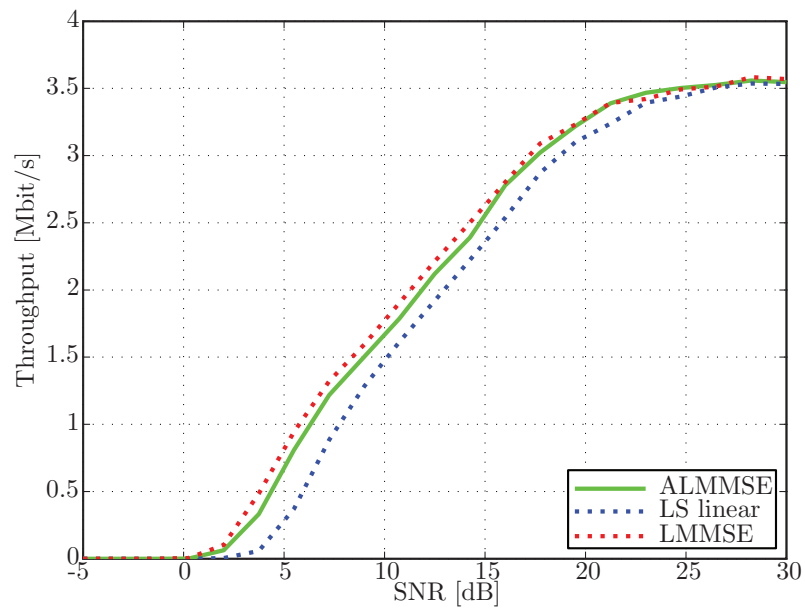


Figure 4.11: Throughput for the ALMMSE estimator



## Chapter 5

# Conclusions and Further Work

This master thesis treats channel estimation for Long Term Evolution (LTE) and investigates the performance of some applicable concepts. It is possible to apply most of the discussed concepts to other Orthogonal Frequency Division Multiplexing (OFDM) systems with slight formal changes. First, I investigated channel estimation for slowly changing channels, where I assumed that the channel stays constant during the transmission of one subframe. Second, I investigated channel estimation for rapidly changing channels.

If no statistical knowledge about the channel is available, for both, block and fast fading, first the Least Squares (LS) channel estimate on the pilot symbol positions has to be calculated. The data channel coefficients have to be obtained by interpolation. The linear interpolation shows the best performance among the presented interpolation techniques, and the lowest computational complexity. Therefore, in case of the LS channel estimation, the linear interpolation should be used. However, one should be aware of edge effects of the linear interpolator at low Signal to Noise Ratio (SNR) values. The SNR loss of a system using the LS estimator with linear interpolation to the system with perfect channel knowledge is approximately 2 dB.

To improve the performance of the LS estimator, the Linear Minimum Mean Square Error (LMMSE) estimator can be implemented by filtering the LS estimate. If the channel autocorrelation is known perfectly, the SNR loss to the system with perfect channel knowledge becomes approximately 0.5 dB. In practice, however, the channel autocorrelation has to be estimated. Such a system is losing approximately 1 dB to the system with perfect channel knowledge. To estimate the channel autocorrelation matrix, the LS channel estimate can be used. Already after few channel realizations, the estimator is performing well. In case of fast fading, also the time correlation has to

be estimated. In the thesis, I show that the LMMSE estimator is robust against wrong temporal statistics. A relative estimation error of 20% of the maximum velocity does not influence the system performance significantly.

To reduce the computational complexity of the LMMSE estimator while preserving its performance, low complex alternatives are investigated. In case of block fading, I discuss an Approximate Linear Minimum Mean Square Error (ALMMSE) estimator, which exploits only the correlation between the  $L$  closest subcarriers instead of the correlation between all subcarriers as in the case of the LMMSE estimator. With increasing  $L$ , the performance is approaching the performance of the LMMSE estimator, and at the same time the computational complexity is increasing. This fact allows adjusting the performance and complexity of the estimator to achieve a good trade-off. In case of fast fading, I propose a novel channel estimator, which makes use of the structure of the channel autocorrelation matrix. The SNR loss to the system using the LMMSE estimator is approximately 0.1 dB.

For LTE, it is found that the block fading assumption is justified up to a maximum velocity of about 20 km/h. Since with increasing velocity the channel changes during the transmission of one OFDM symbol, the subcarriers are not perfectly orthogonal to each other and Inter Carrier Interference (ICI) occurs. Due to the ICI, the performance of the system is significantly reduced, when the receiver does not handle ICI. Consequently at higher velocities not just noise power but also ICI power is the limiting factor of the LTE system.

# Appendix A

## Acronyms

<b>3GPP</b>	3rd Generation Partnership Project
<b>ALMMSE</b>	Approximate Linear Minimum Mean Square Error
<b>A/D</b>	Analog/Digital
<b>DFT</b>	Discrete Fourier Transform
<b>FFT</b>	Fast Fourier Transform
<b>GSM</b>	Global System for Mobile communications
<b>H-ARQ</b>	Hybrid Automated Repeat Request
<b>ICI</b>	Inter Carrier Interference
<b>INTHFT</b>	Institute of Communications and Radio-Frequency Engineering
<b>IFFT</b>	Inverse Fast Fourier Transform
<b>LS</b>	Least Squares
<b>LTE</b>	Long Term Evolution
<b>LMMSE</b>	Linear Minimum Mean Square Error
<b>MIMO</b>	Multiple Input Multiple Output
<b>MSE</b>	Mean Square Error
<b>OFDM</b>	Orthogonal Frequency Division Multiplexing
<b>SINR</b>	Signal to Interference and Noise Ratio
<b>SIR</b>	Signal to Interference Ratio
<b>SISO</b>	Single Input Single Output
<b>SMS</b>	Short Message Service
<b>SNR</b>	Signal to Noise Ratio
<b>T-F</b>	Time-Frequency
<b>UE</b>	User Equipment
<b>WAP</b>	Wireless Application Protocol
<b>WiMAX</b>	Worldwide Inter-operability for Microwave Access
<b>W-CDMA</b>	Wideband Code Division Multiple Access

# Bibliography

- [1] H. Eriksson, “**One global standard**,” January 2009. [Online]. Available: <http://www.ericsson.com/solutions/video/2009/q1/090123-one-global-standard.shtml>
- [2] I. Gartner, “**Gartner says worldwide mobile phone sales declined 8.6 per cent and smartphones grew 12.7 per cent in first quarter of 2009**,” May 2009. [Online]. Available: <http://www.gartner.com/it/page.jsp?id=985912>
- [3] 3GPP, “**Evolved Universal Terrestrial Radio Access (E-UTRA); Physical channels and modulation**,” 3rd Generation Partnership Project (3GPP), TS 36.211, Sept. 2008. [Online]. Available: <http://www.3gpp.org/ftp/Specs/html-info/36211.htm>
- [4] E. Dahlman, S. Parkvall, J. Skold, and P. Beming, **3G Evolution**. Academic Press, July 2007.
- [5] A. Wilzeck and T. Kaiser, “**Antenna subset selection for cyclic prefix assisted MIMO wireless communications over frequency selective channels**,” *EURASIP J. Adv. Signal Process*, vol. 2008, pp. 1–14, 2008, doi: <http://dx.doi.org/10.1155/2008/716826>.
- [6] D. Tse and P. Viswanath, **Fundamentals of Wireless Communication**. Cambridge University Press, June 2005.
- [7] J. J. van de Beek, O. Edfors, M. Sandell, S. K. Wilson, and P. O. Borjesson, “**On channel estimation in OFDM systems**,” in *Proc. IEEE 45th Vehicular Technology Conference (VTC 1995)*, vol. 2, pp. 815–819, 1995, doi: 10.1109/VETEC.1995.504981. [Online]. Available: <http://dx.doi.org/10.1109/VETEC.1995.504981>
- [8] N. Sun, T. Ayabe, and T. Nishizaki, “**Efficient spline interpolation curve modeling**,” in *Proc. Third International Conference on Intelligent Information Hiding and Multimedia Signal Processing, 2007 (IIHMSP 2007)*, vol. 2, pp. 59–62, Nov. 2007, doi: 10.1109/IIHMSP.2007.4457653.
- [9] J. Lei, C. Dazhong, and H. Chunping, “**Two novel transform domain estimation methods for OFDM system and their application environment**,” in *Proc. Canadian Conference on Electrical and Computer Engineering (CCECE 2004)*, vol. 1, pp. 377–380 Vol.1, May 2004.
- [10] C. Oestges, “**Validity of the kronecker model for MIMO correlated channels**,” in *Proc. IEEE 63rd Vehicular Technology Conference (VTC 2006)*, vol. 6, pp. 2818–2822, May 2006, doi: 10.1109/VETECS.2006.1683382.

- [11] C. Mehlführer, S. Caban, and M. Rupp, “**An accurate and low complex channel estimator for OFDM WiMAX,**” in *Proc. Third International Symposium on Communications, Control, and Signal Processing (ISCCSP 2008)*, pp. 922–926, St. Julians, Malta, Mar. 2008. [Online]. Available: [http://publik.tuwien.ac.at/files/pub-et\\_13650.pdf](http://publik.tuwien.ac.at/files/pub-et_13650.pdf)
- [12] “**IEEE standard for local and metropolitan area networks part 16: Air interface for fixed broadband wireless access systems,**” Tech. Rep., 2004. [Online]. Available: [http://ieeexplore.ieee.org/xpls/abs\\_all.jsp?arnumber=1350465](http://ieeexplore.ieee.org/xpls/abs_all.jsp?arnumber=1350465)
- [13] C. Mehlführer, M. Wrulich, J. C. Ikuno, D. Bosanska, and M. Rupp, “**Simulating the long term evolution physical layer,**” in *Proc. of the 17th European Signal Processing Conference (EUSIPCO 2009)*, Glasgow, Scotland, Aug. 2009.
- [14] ITU, “**Recommendation ITU-R M.1225: Guidelines for evaluation of radio transmission technologies for IMT- 2000 systems,**” International Telecommunication Union, Recommendation ITU-R M.1225, 1998.
- [15] R. J. Renka, “**Algorithm 624: Triangulation and interpolation at arbitrarily distributed points in the plane,**” *ACM Trans. Math. Softw.*, vol. 10, no. 4, pp. 440–442, 1984, doi: <http://doi.acm.org/10.1145/2701.356108>.
- [16] J. Liu, K. Liu, and X. Feng, “**Electronic chart based ocean environment development method and its application in digital AUV platform,**” in *Proc. International Symposium on Underwater Technology (UT 2004)*, pp. 423–429, April 2004, doi: 10.1109/UT.2004.1405637.
- [17] D. T. Sandwell, “**Biharmonic spline interpolation of GEOS-3 and SEASAT altimeter data,**” *Geophysical Research Letters*, vol. 12, no. 2, pp. 139–142, February 1987.
- [18] T. K. Moon and W. C. Stirling, **Mathematical Methods and Algorithms for Signal Processing.** Upper Saddle River, NJ: Prentice Hall, 2000.
- [19] Y. R. Zheng and C. Xiao, “**Simulation models with correct statistical properties for Rayleigh fading channels,**” *IEEE Transactions on Communications*, vol. 51, no. 6, pp. 920–928, June 2003, doi: 10.1109/TCOMM.2003.813259.
- [20] T. Zemen and C. Mecklenbrauker, “**Time-variant channel estimation using discrete prolate spheroidal sequences,**” *IEEE Transactions on Signal Processing*, vol. 53, no. 9, pp. 3597–3607, Sept. 2005, doi: 10.1109/TSP.2005.853104.
- [21] A. Stamoulis, S. Diggavi, and N. Al-Dhahir, “**Intercarrier interference in MIMO OFDM,**” *IEEE Transactions on Signal Processing*, vol. 50, no. 10, pp. 2451–2464, Oct 2002, doi: 10.1109/TSP.2002.803347.
- [22] S. Diggavi, N. Al-Dhahir, and A. Stamoulis, “**Intercarrier interference in MIMO OFDM,**” in *Proc. IEEE International Conference on Communications (ICC 2002)*, vol. 1, pp. 485–489, 2002, doi: 10.1109/ICC.2002.996901.